Deltares

TKI verbeteren zettingsprognose

TKI verbeteren zettingsprognose

Client	TKI
Contact	
Reference	
Keywords	creep, soft soils, organic soils, initial strain rate, small loading steps

Document control	
Version	0.1
Date	24-11-2022
Project nr.	11203922-004
Document ID	11203922-004-GEO-0003
Pages	63
Classification	
Status	preliminary This is a preliminary report, intended for discussion purposes only. No part of this report may be relied upon by either principal or third parties.

Author(s)		
	M. Konstantinou	
	C. Zwanenburg	

Doc. version	**Author**	**Reviewer**	**Approver**	**Publish**
0.1	C. Zwanenburg			

Summary

Over the last decades the use of isotachs in settlement prediction has found its way in the practice of daily engineering. In January 2019 an expert meeting was held to discuss the status of settlement prediction in Dutch practice. It was concluded that for large embankments, for which the stress condition in the sub soil is pushed beyond the initial yield stress, accurate and reliable predictions could be made using the isotach principle. This observation is supported by findings in international literature, e.g. Nash & Brown (2015).

However, for small load increments, for which the stress conditions remain below the initial yield stress, the general consensus was that the present prediction methods are in-accurate. This in-accuracy resulted in wrong conclusions regarding the expected settlement and in extra construction or maintenance costs.

A further analysis of the problem shows that the prediction of settlement due to a small load increment strongly depends on the initial conditions, like initial strain rate, OCR or yield stress. For a large load increment, that pushes soil conditions into the normally consolidated state, initial conditions are no longer relevant when predicting settlement. As such the accuracy and reliability of the predicted settlement for large load increments seems better than for small load increments.

Establishing the initial conditions not only requires accurate measurement of the yields stress, OCR or initial strain rate, but also demands a model that can predict strain rate correctly. The literature review presented in this report discusses the recent insights in the origin and prediction of creep strain rates for over consolidated conditions. Non-linearity in isotachs causes the distance between the isotachs to decrease at decreasing strain rates. While at present the models used in Dutch engineering practice assume an evenly spaced isotachs, non-linear isotachs will predict a more rapid decline in strain rate during aging or unloading. An opposite trend is found by a distortion of isotachs due to soil structure change induced by unloading and corresponding swelling. When accounting for distortion of the isotachs a larger strain rate after unloading is found then would be found if distortion of the isotachs is not accounted for. Besides non-linearity and distortion of the isotachs, an internal state variable can be used to describe a gradual acceleration of creep to a target value when load steps are applied, and creep is activated. The literature review in this report discusses different implementations of these concepts in constitutive models.

The literature review mainly reflects behaviour which is found from tests on silty clays. Organic soils are more relevant for Dutch practice when it comes to settlement prediction. Additional experiments and field data are needed to establish the applicability of the outcome of the literature review for organic soils.

Contents

1 Introduction

1.1 TKI “verbeteren zettingsprognose”

In geotechnical design prediction of sub soil deformations during the lifetime of a construction forms an important design aspect. Already in the early days of soil mechanics the complexity of sub soil deformation, particular the long-term settlement, was acknowledged. An important step forward was made by the introduction of the isotach concept. The isotach concept developed over time and formed the basis of several tools for settlement prediction of embankments on compressible soil.

In Dutch engineering practice, isotach models have become a valuable tool for settlement prediction. In an expert meeting, held at Deltares January 2019, it was generally acknowledged that the present use of isotach models works well for large embankments which weight exceed the initial yield stress in the sub soil below the embankment. For small loadings however, prediction of settlement was considered to be less accurate. Based on this observation, the research project TKI – verbeteren zettingsprognose is established. The research project is dedicated to validating the use of isotach models for small loadings. In the context of this study, a small loading refers to is a load increment that remain below the initial yield stress of the loaded soil.

This report summarizes a literature study on isotach models and compares the latest developments to the isotach models that are typically used in Dutch engineering practice.

1.2 Aim of the study

This study aims to improve the predictability of the sub soil settlement due to small load increments. Small load increments are defined here as increments for which the stress condition after application of the loading remains below the initial yield stress. To reach this aim, this study will:

- Lay down comparisons between model predictions, of existing models and measurements of laboratory and field data. This provides insight in the efficiency of current models to predict settlement due to a small load increment.
- Literature study on the latest developments in settlement prediction. The literature study will show if new developments are available that could be used to further improve settlement prediction for small load increments
- Provide recommendations to improve settlement prediction for small load increments in daily engineering.

1.3 Report set-up

This report first describes the present working procedure in settlement prediction. It is acknowledged that in the daily practice, within the different available guidelines, a variety of working procedures are applied. These working procedures include differences in implementation of the isotach principle. Chapter 2 describes a typical implementation of the isotach principle. This description is used as the reference implementation against which possible consequences of new developments are studied. Chapter 2 also includes an illustration of the problems encountered when applying the reference implementation. Chapter 2 follows further with a literature study. Chapter 3 discusses some aspects of the new models proposed in literature. Chapter 4 finalizes with a summary and suggestions for the next steps in the research project TKI – verbeteren zettingsprognose.

2 Literature study

2.1 Introduction

The isotach concept originally proposed by Suklje (1957) and further introduced, by among others Bjerrum (1967), is used in practice for the evaluation of 1D compression. The classical isotach concept is visualized in Figure 2-1 from Bjerrum (1967). In the stress – strain space lines of equal strain rate are defined. These lines are referred to as isotachs and in the classical approach the lines representing a 10-fold difference in strain rate have an equal mutual distance. The isotachs represent a unique combination of strain, vertical effective stress and strain rate, which remains valid during the entire compression process.

Since its development, several models based on the isotach concept have been developed, as discussed below. This literature study aims in identifying and summarizing the latest developments in material models for predicting creep settlement based on an isotach elasto-viscoplastic (EVP) framework.

2.2 Present situation

2.2.1 Reference implementation

The implementation of the isotach model which is used as a reference in this study complies with the implementation used in the software D-Settlement (Deltares 20?). This implementation is based on the work by Den Haan (Den Haan, 1992, 1994, 1999; Den Haan & Edil, 1994; Den Haan & Selmeijer, 2000) and summarised by Visschedijk, 2010. The following text is taken from Zwanenburg (2021).

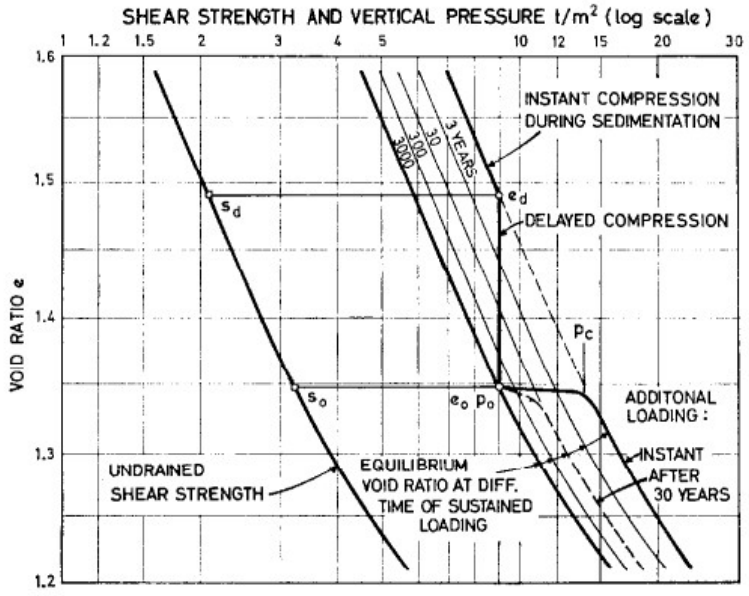

Figure 2-1, The isotach concept from Bjerrum (1967)

Figure 2-1 shows a compression curve during sedimentation in which a soil layer develops. At some point the sedimentation process stops. However, settlement continues due to creep, in Figure 2-1 referred to as delayed compression. When time progresses the creep strain rate slows down, as predicted by equation (0.1); the creep strain in Figure 2-1 which develops

between 3 years and 30 years is the same as between 30 years and 300 years, however the time required to reach this amount of strain is 10-times longer. The same holds for the strain developed between 300 years and 3000 years, etc.

The lines representing age, 3 years, 30 years etc. are running parallel to the instant compression line. Independent from the stress level to which the load was raised, after a 3-year creep the combination of strain and log(σ'_v) is such that it falls on the 3-year line. The same holds for the 30, 300- and 3000-year line. The creep strain rate follows from the time derivative of the creep strain, ε_c. Equation (0.1) shows that the lines representing age are also lines of constant strain rate;

$$\varepsilon_s = C_\alpha \log\left(\frac{\tau_2}{\tau_1}\right)$$
$$\frac{d\varepsilon_s}{d\tau} = \frac{d}{d\tau}\left(C_\alpha \log\left(\frac{\tau_2}{\tau_1}\right)\right) = \frac{C_\alpha}{\ln(10)}\frac{\tau_1}{\tau_2} = \frac{C_\alpha}{2.3\,\tau} \qquad (0.1)$$

In which:

τ_1, τ_2 = the start and end time for the period for which creep strain is evaluated.
C_α = creep parameter
ε_s = creep strain

For τ_1 = 1 day, τ represents the creep period or the age in Figure 2-1. Then, equation (0.1) shows that the strain rate is constant along the line representing a specific age. This explains their name; isotach is Greek for constant velocity.

Intrinsic time, τ

Figure 2-2 sketches the isotachs in more detail. In analysing laboratory testing data expressing time in days might be more relevant than years and consequently Figure 2-2 sketches the 1, 10, 100 and 1000 day compression line. Not only time causes the soil conditions to move from one isotach to the other. Also, loading and unloading steps will cause acceleration or a slowdown of the creep strain rate. This is shown by Figure 2-2. A soil being loaded to point *a* in Figure 2-2 and then allowed to creep for 100 days reaches point *b* and has a corresponding creep strain rate. If, after the 100-day creep period, the soil is loaded to point *c*, which is on the 10-day compression line, the creep strain rate increases and is equivalent to a strain rate that would be found after a 10-day creep period. Alternatively, if, when reaching point *b*, the soil is unloaded to point *d,* the creep strain rate drops and will be equivalent to the strain rate that would be found after a 1000-day creep period.

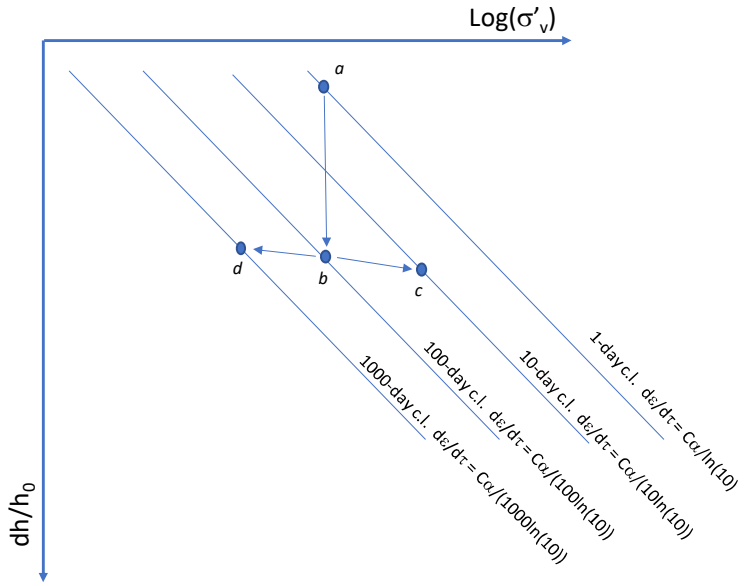

Figure 2-2, Influence loading and unloading on creep strain rate and intrinsic time

In construction or laboratory testing, the time *t* is set to zero when a load increment is applied. From this moment there are two timescales. The first timescale represents the time scale according to which creep develops. The second timescale represents the construction or laboratory testing time, *t*, with *t* = 0 the start of the loading. To be able to account for this difference, the concept of intrinsic time, τ is introduced (den Haan & Edil, 1994). The intrinsic time τ of a soil refers to the isotach which represents the stress – strain – strain rate conditions of the soil. The intrinsic time τ for point *a* in Figure 2-2 is 1 day, for point *b* 100 days etc.

For the first step in an oedometer test τ is typically large. After all, when retrieving the soil sample from the field, the sample was (strongly) unloaded. The small first loading step typically keeps the stress – strain conditions well below the 1-day compression line, with consequently a large τ. During the oedometer test the time, *t*, is measured, with *t* = 0 s at the application of the first load step. Consequently, there is a clear difference between the intrinsic time, τ and the loading time or test time, *t*. Only when large loading steps are applied, which clearly brings the soil conditions beyond the 1-day compression line, the difference between the test time *t* and the intrinsic time, τ becomes negligible.
In elaborating laboratory test data, the time - settlement curve is typically presented as a function of the test time, *t* and the intrinsic time τ is not determined. The creep strain development, as given by equation (0.1) follows the intrinsic time, τ. By plotting creep strain as a function of test time *t* instead of intrinsic time τ causes a shift of the time – settlement curve. This is a constant shift:

$$t = \tau + t_r \tag{0.2}$$

In which:

- t = loading time, typically set to zero when loading starts, or a load increment has been applied
- τ = intrinsic time; the time scale according to which the soil is creeping
- t_r = time shift

Due to the use of the log-axis when plotting the time-settlement curve the linear relation between creep strain, ε_c and the logarithm of the intrinsic time, log(τ), becomes a non-linear relation between creep strain, ε_c and the logarithm of the loading time, log(*t*). As shown by

Figure 2-3, the time shift t_r has a strong influence for small values for t and a small influence for large values for t. Consequently, the creep index C_α can be determined sufficiently accurate from the ε - log(t) curve when either t_r is small or the loading period is sufficiently long. It should be noted that besides the time shift t_r, consolidation also accounts for initial non-linearity in the ε - log(t) curve.

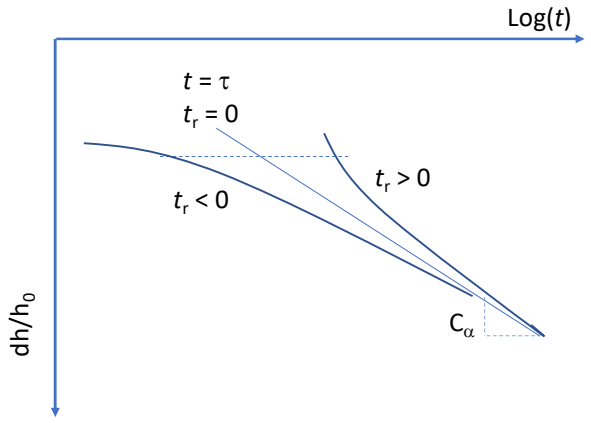

Figure 2-3 Influence of time shift, t_r on the time – development of soils.

The influence of loading and unloading on the intrinsic time

Figure 2-2 shows that loading and unloading causes changes in the intrinsic time. Loading results in a creep rate increase, which according to equation (0.1), corresponds to a reduction in intrinsic time, τ. While unloading results in a creep rate decrease and according to equation (0.1) to an increase in τ. A mathematical expression linking a load increment to the change in intrinsic time follows from Figure 2-4.

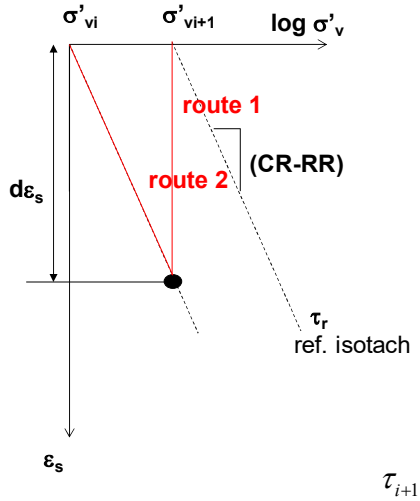

route 1: $d\varepsilon_s = C_\alpha \log\left(\frac{\tau_{i+1}}{\tau_i}\right)$

route 2: $d\varepsilon_s = (CR-RR)\log\left(\frac{\sigma'_{v,i+1}}{\sigma'_{v,i}}\right)$

$$d\varepsilon_{s,1} = d\varepsilon_{s,2}, \quad C_\alpha \log\left(\frac{\tau_{i+1}}{\tau_i}\right) = (CR-RR)\log\left(\frac{\sigma'_{v,i+1}}{\sigma'_{v,i}}\right),$$

$$\log\left(\frac{\tau_{i+1}}{\tau_i}\right)^{C_\alpha} = \log\left(\frac{\sigma'_{v,i+1}}{\sigma'_{v,i}}\right)^{(CR-RR)},$$

$$\tau_{i+1} = \tau_i \left(\frac{\sigma'_{v,i+1}}{\sigma'_{v,1}}\right)^{\frac{CR-RR}{C_\alpha}} \tag{0.3}$$

Figure 2-4 Relation between load increment and intrinsic time increment

Equation (0.3) can be used to obtain the intrinsic time prior to loading; the initial intrinsic time. With the yield stress being the yield point on the reference isotach, which corresponds to $\tau = \tau_0 = 1$ day and the initial vertical effective stress given by σ'_v, follows:

$$\tau = \tau_0 \left(\frac{\sigma'_{vy}}{\sigma'_v}\right)^{\frac{CR-RR}{C_\alpha}} = \tau_0 OCR^{\frac{CR-RR}{C_\alpha}} \tag{0.4}$$

In which:

RR = re-compression index
CR = compression index
C_α = creep parameter
τ_0 = intrinsic time reference isotach; τ = 1 day
σ'_{vy} = yield stress related to reference isotach
OCR = over consolidation ratio.

The isotach model in predicting settlement
The concept of intrinsic time allows for an efficient settlement prediction especially when settlement due to a succession of loading, unloading and re-loading steps are applied, (Visschedijk, 2010). The scheme is elaborated in 5 steps, as shown by Figure 2-5.

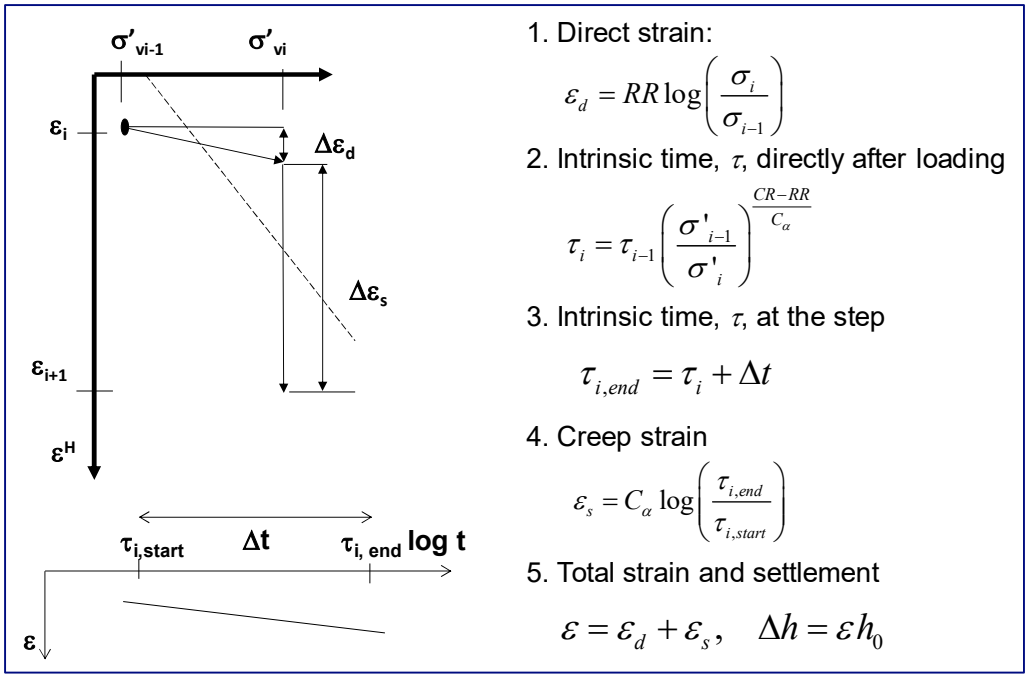

Figure 2-5 Calculation procedure

The first step determines the direct strain using the recompression index, *RR* and the total load step. The second step uses the intrinsic time principle to derive the intrinsic time, τ directly after the load application. The third step determines the intrinsic time, $\tau_{I,end}$, at the end of the step. Step 4 applies equation (0.1) to derive the creep strain that develops during the step. Finally, step 5 calculates the total strain, ε, by summing the direct strain, ε_d, and creep strain, ε_s, and calculates the settlement.

The yield stress is not mentioned directly in Figure 2-5. However, the yield stress, or OCR, is required to estimate the initial intrinsic time and therefore, position the initial conditions to the reference isotach. Figure 2-5 is well suited for a step wise procedure, in which the final conditions in terms of effective stress and intrinsic time form the initial conditions of the next step.

2.2.2 Linear and natural strain

Soil layers in situ and soil specimen in laboratory tests will have a finite thickness. Even after large deformation, their thickness will not reduce to zero irrespective of the load level. Consequently, the ε - log(σ'_v) will not be linear at large strain and compression ratios, based on linear strain, will not be constant. To deal with the non-linearity at large strain a different strain measure is introduced.

The conventional engineering strain, also referred to as linear or Cauchy strain, ε^C relates deformation to the initial dimensions:

$$\varepsilon^C = \frac{\Delta h}{h_0} \tag{0.5}$$

In which:

ε^C = Cauchy strain or engineering strain
Δh = change in layer thickness or specimen height in laboratory testing
h_0 = original layer thickness or specimen height in laboratory testing

The natural strain or Henky strain, ε^H relates the increment in layer thickness or specimen height in laboratory testing, dh, to the actual height, h. Since the actual height is constantly changing ε^H contains the summation of infinitesimal increments, dh, related to their actual sample height, h:

$$\varepsilon^H = \int_{h=h_0}^{h=h_0-\Delta h} \frac{dh}{h} = -\ln\left(\frac{h_0 - \Delta h}{h_0}\right) = -\ln\left(1 - \varepsilon^C\right) \tag{0.6}$$

In which:

ε^H	= natural strain
ε^C	= linear strain
dh	= infinitesimal incremental change in height, h
h	= sample or layer thickness,
h_0	= initial sample or layer thickness
Δh	= total change in sample or layer thickness

Figure 2-6 illustrates the differences between the two strain measures. For linear strain a constant increase in strain with increasing reduction in layer thickness is found. For $\varepsilon^C = 0$, the layer thickness is compressed to 0, which is physically impossible. For natural strain ε^H goes to infinity when the layer thickness reaches 0.

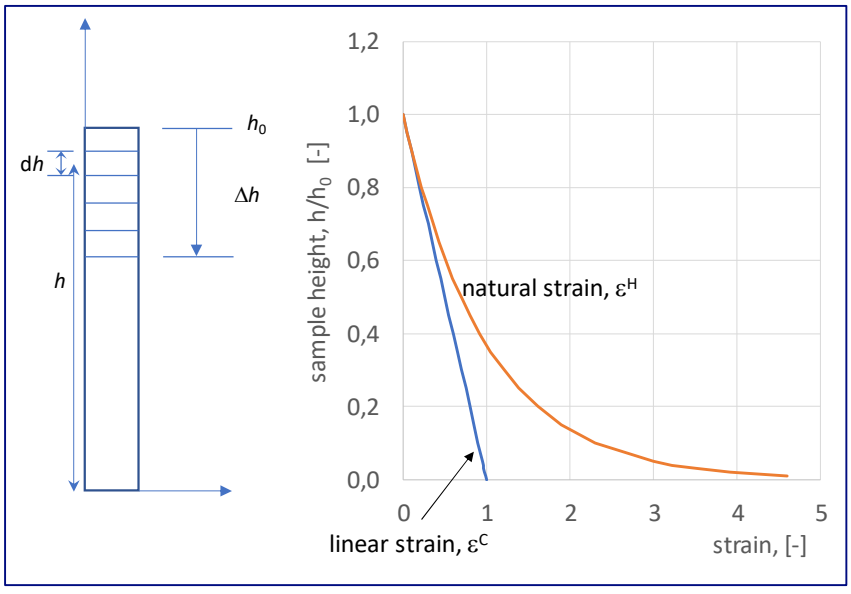

Figure 2-6, Linear and natural strain

Figure 2-7 shows the results of an incremental loading test, IL, on a peat sample. The results are plotted against linear and natural strain. The difference between the two strain definitions are negligible for a strain level up to $\varepsilon = 0.2$. For a strain level beyond $\varepsilon^C = 0.5$, the linear strain measure starts to bend as the sample behaviour stiffens due to a final sample thickness. For the loading steps beyond $\varepsilon^C = 0.5$, the compression ratio, CR is no longer constant and reduces for increasing strain. The natural strain develops linear for $\log(\sigma'_v)$ even at large strain.

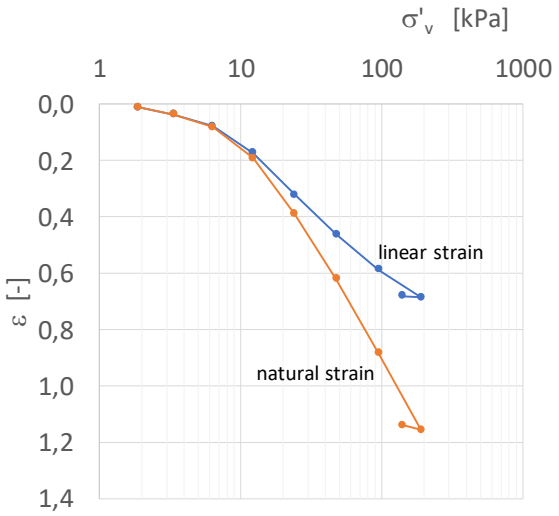

Figure 2-7 Results of an Incremental loading test on peat plotted for linear and natural strain, properties of the tested material, saturated weight, γ_w = 10 kN/m³, water content, w *= 1124 %, loss on ignition, LOI = 87%.*

2.2.3 Illustration of the problem

The research problem is illustrated by a series of 9 Incremental Loading oedometer tests on peat samples from location Zegveld. Table 2-1 presents the applied loading scheme. The loads were kept constant for 24 hours except for loading step 2 en 10 where the load was maintained for 168 hours (7 days). The load applied in step 2 was well below the natural yield stress and is used to investigate the creep rates in the over consolidated region. The load applied in step 10 is well beyond the natural yield stress and shows the creep characteristics for normally consolidated conditions. Details of the tested specimen, the test results and analysis are presented in appendix A.

Creep strain rates, at the end of step 2 and step 10, were predicted using the reference implementation and compared to the measured creep strain rates. Since the compression indices as well as the yield stress were determined for each of the individual specimen in the same test as the strain rates were determined, the influence of natural variability could be excluded.

Table 2-1, Loading scheme

Load step	Load [kPa]	Duration [days]
1	2	1
2	5	7
3	7	1
4	10	1
5	15	1
6	20	1

7	40	1
8	20	1
9	40	1
10	80	7
11	140[b]	1

[a] The first load step is used as reference to determine the initial height.
[b] Test 65 is the only exception: a load of 122 kPa was applied during the last load step.

Table 2-2, Comparison of measured and predicted creep strain rates at the end of load step 10

Test nr	C_α [-]	τ [days]	$\dot{\varepsilon}^C_{theory}$ [10^{-8} 1/s]	$\dot{\varepsilon}^C_{measured}$ [10^{-8} 1/s]
9	0.0384	7	2.76	2.75
55	0.0306	7	2.20	2.19
99	0.0470	7	3.37	3.36
67	0.0411	7	2.95	2.94
97	0.0417	7	2.99	2.98
25	0.0322	7	2.31	2.30
26	0.0323	7	2.32	2.31
42	0.0305	7	2.19	2.19
65	0.0363	7	2.61	2.59

Table 2-2 shows the comparison of the creep strain rates at the end of load step 10. The predicted creep strain rates, $\dot{\varepsilon}^C_{theory}$ are derived by using equation (0.1). In step 10, the load condition is pushed beyond the 1-day compression line and the intrinsic time, τ, is approximately equal to the duration of the load step, 7 days. The measured strain rate, $\dot{\varepsilon}^C_{measured}$ is assessed by curve fitting the ε - log(t) plot of step 10. Taking the derivative of the best fit and evaluating the derivative at the end of the load step provides the measured strain rate. Table 2-2 shows a very good comparison between $\dot{\varepsilon}^C_{measured}$ and $\dot{\varepsilon}^C_{theory}$. Details of the analysis are provided by appendix A.

For loading step 2, the creep strain rates are predicted by first evaluating the intrinsic time, τ_{start}, directly after unloading, by equation (0.4). The summation of τ_{start} and the duration of the load step provides the intrinsic time at the end of the load step, τ_{end}. Applying τ_{end} to equation (0.1) yields the predicted strain rate at the end of step 2. The value for $\dot{\varepsilon}^C_{measured}$ in step 2 is evaluated following the same procedure as applied for step 10.

Table 2-3, Comparison between measured and predicted creep strain rate for step 2

Test nr	OCR [-]	(CR-RR)/Cα [-]	τ_{start} [days]	$\dot{\varepsilon}^C_{theory}$ [1/s]	$\dot{\varepsilon}^C_{measured}$ [1/s]
9	2.5	10.55	13781	$1.40\ 10^{-11}$	$3.68\ 10^{-9}$
55	3.1	18.70	$1.34\ 10^{9}$	$1.15\ 10^{-16}$	$7.24\ 10^{-10}$

99	1.8	6.87	65	$3.64\ 10^{-9}$	$1.60\ 10^{-8}$
67	2.2	7.13	253	$8.17\ 10^{-10}$	$1.11\ 10^{-8}$
97	2.2	7.01	253	$8.28\ 10^{-10}$	$8.97\ 10^{-9}$
25	1.8	12.23	1663	$9.73\ 10^{-11}$	$5.47\ 10^{-9}$
26	2.1	12.28	8059	$2.01\ 10^{-11}$	$3.60\ 10^{-9}$
42	2.7	14.99	2315795	$6.63\ 10^{-14}$	$2.35\ 10^{-9}$
65	2.3	9.39	2270	$8.03\ 10^{-11}$	$5.82\ 10^{-9}$

Table 2-3 shows that the predicted and measured creep strain rates differ by several orders in magnitude. The reference implementation seems to underestimate the creep strain rate by a factor 20 – 200 and even more for tests 55 and 42.

Table 2-3 also shows the large variability in the parameters, OCR and (CR-RR)/C_α that determine the initial conditions. The OCR, in Table 2-3, has a mean value of 2.3 with a coefficient of variation, CV of 0.18. The ratio (CR-RR)/C_α has a mean value of 11 with CV = 0.36. The variation in these parameters and the strong non-linearity in equation (0.4) results in a large scatter in τ_{start}, which varies from 65 days, in test 99, to 1 340 000 000 days, in test 55. Consequently, a large scatter in predicted creep strain rate if found. However, the predicted creep strain rate is in the order of 10^{-10} to 10^{-11} 1/s or lower. The measured creep strain rates are in the order of 10^{-8} to 10^{-9} 1/s. This shows that the differences between measured and predicted creep strain rates is not only explained by the scatter in OCR and (CR-RR)/C_α.

Section 1.1 refers to an expert meeting at the start of this project. In this meeting the feeling was shared that the reference implementation works well for large loading, that pushes sub soil conditions into the normally consolidated region and seems to be less accurate for small loading steps. The results of the analysis above seem to support that feeling. The comparison of predicted and measured strain rates after 7 days for initially normally consolidated conditions is remarkably good. However, for over consolidated conditions, the creep strain rate is underpredicted by an order in magnitude of 20 to 200. Parameter uncertainty contributes to observed differences but does not fully explain these differences. This indicates that a further development of the implementation if the isotach concept is needed to improve the ability to predict creep strain rates after small loading steps.

2.2.4 Remarks

The next sections discuss the literature review on the latest developments related to prediction of creep strain. In the discussion of the latest development the following remarks should be considered:

Remark 1, reference implementation
Section 2.2.1 gives the implementation that is used as the reference in this study. In daily engineering minor changes to this implementation might be used.

It is acknowledged that geometrical non-linearities play a role, especially when evaluating behaviour of soft soils, like organic clays and peats. However, in this study the implementation based on linear strain, section 2.2.1, is selected as reference. The implementation based on linear strain does not differ conceptually from the implementation based on natural strain and is more straight forward to apply and therefore suits better as a reference.

It should be noted that the implementation based on natural strain, as developed by Den Haan (1992, 1994, 1999) uses the natural logarithm, *ln*, in the stress – strain and time – strain relations.

Remark 2; definition compression ratio CR

Two different approaches are used in division of total strain in a direct and visco-plastic component and corresponding definition of the compression ratio, CR. Visco plastic strain is defined as the difference between total strain and direct strain according to equation (0.7).

$$\varepsilon^{p} = \varepsilon - \varepsilon^{d} \tag{0.7}$$

In which:

$\varepsilon, \varepsilon^{d}, \varepsilon^{p}$ = Strain, direct strain and plastic strain respectively

In approach 1, (e.g. Yuan & Whittle, 2018 or Watabe et al., 2012) the compression ratio, CR is directly related to the visco plastic strain, equation (0.8).

$$\varepsilon^{p} = CR \log\left(\frac{\sigma'_{v,u}}{\sigma'_{vy}}\right) + C_{\alpha} \log\left(\frac{\tau}{\tau_{0}}\right) \tag{0.8}$$

In which:

CR = Compression ratio for normally consolidated behaviour

RR = Compression ratio for re-loading conditions

$\sigma'_{v,u}$ = Vertical effective stress after consolidation

σ'_{vy} = Yield stress

τ = Intrinsic time

τ_{0} = Reference intrinsic time, typically, τ_{0} = 1 day.

Consequently, to derive the value for the compression ratio from laboratory tests, the measured total strain needs to be corrected for the direct strain, according to equation (0.7), which can only be estimated numerically.

In approach 2, (e.g. Den Haan, 1992, 1999), the compression ratios are related to total strain and correction of measurement data is required to obtain the parametric value for these ratios. Consequently, the expression for the visco plastic strain component turns into:

$$\varepsilon^{p} = \left(CR - RR\right) \log\left(\frac{\sigma'_{v,u}}{\sigma'_{vy}}\right) + C_{\alpha} \log\left(\frac{\tau}{\tau_{0}}\right) \tag{0.9}$$

When applied correctly, calculated settlement using these equations should provide the same result. However, since the numerical value for CR differs, the two approaches should not be mixed. The different approaches have some consequences in the mathematical derivation of the models. This will be discussed in the following sections when relevant.

Tsutsumi & Tanaka (2011) illustrate the difficulty encountered when using approach 1. For most soils the unloading – reloading loop results in a hysteresis in the stress strain curve. Consequently, the reloading stiffness is not uniquely defined and typically reloading stiffness for small unloading is higher than found for larger unloading. Tsutsumi & Takani (2011) determine the unloading stiffness C_c at 20% and 80% unloading and conclude that in the analysis the influence of using the different C_c values is small.

Although in many scientific papers approach 1 is used, authors rarely explain how ε^{p} was derived from total strain, ε.

It should be noted that the reference implementation, section 2.2.1, uses approach 2.

Remark 3; the use of intrinsic time

Not all authors seem to acknowledge the concept of intrinsic time, Den Haan & Edil (1994). Some of the discussed changes in C_α after unloading could be explained by the change in intrinsic time that is induced by a shift to the isotach corresponding to a lower strain rate.

Remark 4, the relevance of initial conditions
The assessment of the intrinsic time plays an important role in the calculation procedure given by Figure 2-5. The intrinsic time at the end of the time step, $\tau_{i, end}$ is found by the summation of the intrinsic time direct after the application of the load increment, τ_i, and the time increment Δt. For large loading steps which will bring the soil conditions to the right of the 1-day compression line, τ_i will be small and $\tau_{i, end}$ is nearly equal to Δt. For these large loading steps, errors in the determination of τ_i have no or a negligible influence on $\tau_{i, end}$ and have therefore no of a negligible influence on the settlement prediction. This illustrated by the elaboration of 9 IL tests on peat, as discussed in section 2.2.3.

For small loading steps for which the soil conditions remain left of the 1-day compression line, τ_i will be relatively large. Errors in the determination of, τ_i have an influence on $\tau_{i, end}$ and as such on the settlement prediction. Step 2 from Figure 2-5 calculates τ_i from the conditions in the previous step, τ_{i-1}. When only one loading step is applied or for the first loading step, τ_{i-1} refers to the initial conditions. Consequently, in the prediction of settlement due to a small loading step the initial conditions play an important role; wrongly assessed initial conditions will result in a wrong settlement prediction. As mentioned before, this is clearly different from large loading steps, for which the soil conditions are brought to the right side of the 1-day compression line and the influence of the influence of the initial conditions vanish.

In the validation of the use of isotach models for small load increments, the assessment of initial conditions plays a key role. The initial conditions are given by the initial creep strain rate, initial equivalent age and / or OCR. The assessment of the initial conditions partly follows from the model formulation when it comes to the relation between initial creep strain rate or initial equivalent age and OCR and follows partly from determination of initial stress conditions and yield stress to find OCR.

The literature review described in this report explores the latest developments in model formulation in relation to the prediction of initial conditions.

2.3 Latest developments in EVP formulations in settlement prediction

2.3.1 Introduction to the rate-dependency of the yield stress

Leroueil (2006) discusses the rate dependency of the yield stress. The yield stress is typically defined as the stress level which bounds the elastic, un- and re-loading, region. Typically, the yield stress is obtained from the one-day compression line. When plotting the plastic strain, ε^p - log(σ'_v), the yield stress is found at the intersection of the one day compression line with the horizontal axis. In constant rate of strain, CRS, testing, different loading rates can be applied and the stress – strain conditions can follow different isotachs. Each of these isotachs cross the horizontal axis at a different stress level, resulting in different yield stresses for the different isotachs, see Figure 2-8.

The reference strain rate is typically taken at 1.0×10^{-7} 1/s representing the strain rate found after 24 hours in incremental loading tests for normally consolidated conditions, (Watabe et al. 2012, Watabe & Leroueil, 2015). For lower strain rates lower yield stresses are found, resulting in an increase in yield stress for increasing strain rates.

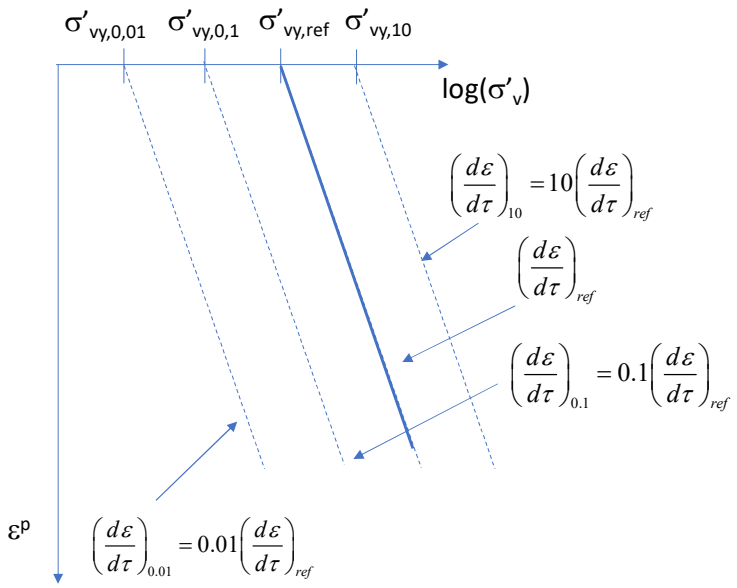

Figure 2-8, Sketch isotachs for different strain rates and corresponding differences in yield stress

The strain rate dependency of the yield stress follows from numerical formulation of the isotach model, as discussed by a.o. Den Haan (1992, 1999), Visschedijk (2010). The creep strain rate is found by differentiating of the creep law:

$$\varepsilon = C_\alpha \log\left(\frac{\tau}{\tau_0}\right); \quad \frac{d\varepsilon}{d\tau} = \frac{1}{\ln(10)}\frac{C_\alpha}{\tau} \tag{0.10}$$

Consequently, the ratio of different strain rates is the reciprocal of the corresponding intrinsic times:

$$\frac{\left(d\varepsilon/d\tau\right)_1}{\left(d\varepsilon/d\tau\right)_2} = \frac{\tau_2}{\tau_1}$$

Den Haan & Sellmeier (2000), Visschedijk (2010) discusses the relation between intrinsic time and stress changes:

$$\tau_2 = \tau_1\left(\frac{\sigma'_{vy,1}}{\sigma'_{vy,2}}\right)^m, m = \frac{CR-RR}{C_\alpha}, \quad \log\left(\frac{\tau_2}{\tau_1}\right) = m\log\left(\frac{\sigma'_{vy,1}}{\sigma'_{vy,2}}\right) \tag{0.11}$$

It should be noted that in the formulation above CR is related to total strain, approach 2 as explained in section 2.1. When applying approach 1, in which the compression index CR is related to the visco plastic strain, *m* in equation (0.11) is reduces to *m* = CR/C_α.

When plotting the ratio $\left(\sigma'_{vy,1}/\sigma'_{vy,2}\right)$ versus $d\varepsilon/d\tau$ in a double logarithmic graph, a line with slope 1/*m* is to be expected. Figure 2-9 shows Figure 18 from Leroueil (2006). For different laboratory and field data, the relation between yield stress and strain rate is shown. The dotted line has a slope α which corresponds to 1/*m*. Despite the scatter, it is concluded in Leroueil (2006) that measurement data deviate from the straight line with slope α or 1/*m*. The consequence of this conclusion is that the measurement data seem to indicate that the isotachs are not equi-distanced. Instead, the isotachs seem to get closer to each other at low strain rates and have larger distances at higher strain rates.

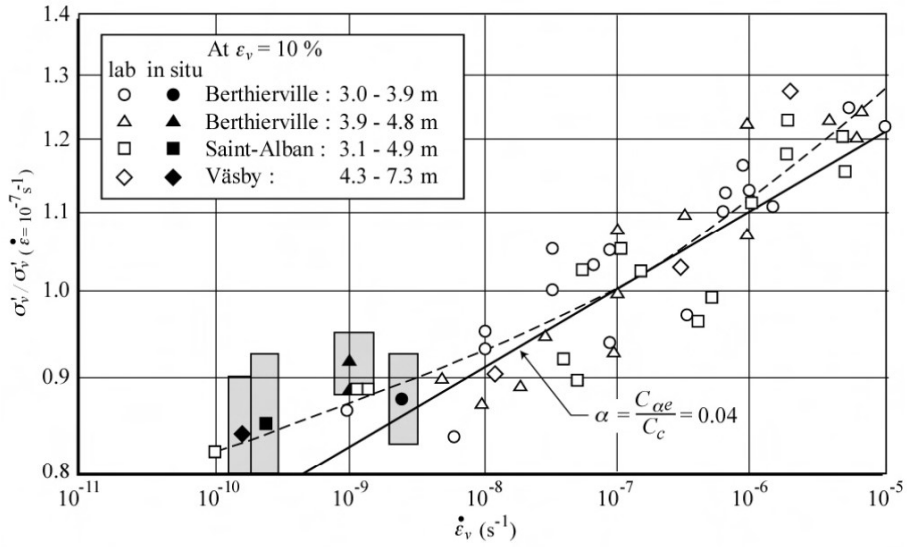

Figure 2-9 Relation between strain rate and yield stress, from: Leroueil, 2006

The strain rate dependency of yield stress is used to normalize stress – strain curves for different soil types, Leroueil (2006), Watabe et al. (2008), Watabe et al. (2012), Watabe and Leroueil (2015).

The one-day compression curve is typically used as a reference compression curve. Normalizing the reference compression curve by the yield stress related to the reference compression curve, results in a (ε_{vp} – $\log\frac{\sigma'_v}{\sigma'_{vy}}$) curve, shown by Eq. (0.12) and Figure 2-10.

$$\frac{\sigma'_v}{\sigma'_{vy}} = f(\varepsilon_{vp}) \qquad (0.12)$$

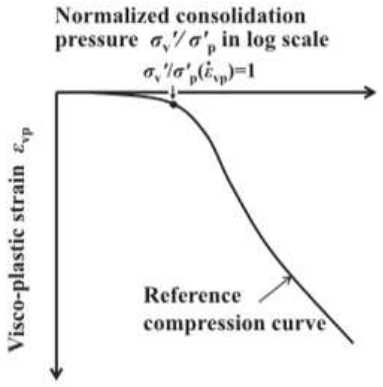

Figure 2-10. Reference compression curve $\left(\varepsilon_{vp} - \log\left(\sigma'_v/\sigma'_{vy}\right)\right)$ *curve, after Watabe & Leroueil 2015* σ'_p *= yield stress,* σ'_{vy}.

Following Watabe et al. (2012) the relation between the yield stress, σ'_{vy}, and strain rate is given by:

$$\ln \frac{\sigma'_{vy} - \sigma'_{vy,L}}{\sigma'_{vy,L}} = c_1 + c_2 \cdot \ln \dot{\varepsilon}_{vp} \qquad (0.13)$$

Where:

c_1 = $\ln\left(\left(\sigma'_{vy} - \sigma'_{vy,L}\right)/\sigma'_{vy,L}\right)$ at $\dot{\varepsilon}_{vp} = 1$

c_2 = strain rate dependency

$\sigma'_{vy,L}$ = lower limit of σ'_{vy}

Watabe et al. (2012) and Watabe & Leroueil (2015) refer to the parameters, c_1, c_2 and $\sigma'_{vy,L}$ as isotach parameters.

It should be noted that by introducing a lower limit for the yield stress, $\sigma'_{vy,L}$, the concept of a zero-strain isotach is accepted. The zero strain isotach is further discussed in section 2.3.2.

Based on Eq. (0.12) and Eq. (0.13), the compressibility of the soil is described by the reference compression curve and the three isotach parameters (c_1, c_2 and $\sigma'_{vy,L}$). For worldwide inorganic clays the authors suggest using a value of $\sigma'_{vy,L}/\sigma'_{vy,0} = 0.7$, $c_1 = 0.935$ and $c_2 = 0.107$. In which, $\sigma'_{vy,0}$ is defined as the σ'_{vy} corresponding to an $\dot{\varepsilon}_{vp}$ value of 1.0×10^{-7} s^{-1}, which is close to the average strain rate obtained in a 24-h incremental loading test. These values have been derived by applying the proposed method on the CRS test results of various clay samples. As can be seen in Figure 2-11 the $\log\left(\sigma'_{vy}/\sigma'_{vy,0}\right)$-$\log \dot{\varepsilon}_{vp}$ relationship for worldwide clays can be adequately described by Eq. (0.13) by applying the recommended isotach parameter values for c_1, c_2 and $\sigma'_{vy,L}$. The red line in this figure corresponds to the integrated curve as calculated based on Eq. (0.13) for $\sigma'_{vy,L}/\sigma'_{vy,0} = 0.7$, $c_1 = 0.935$ and $c_2 = 0.107$.

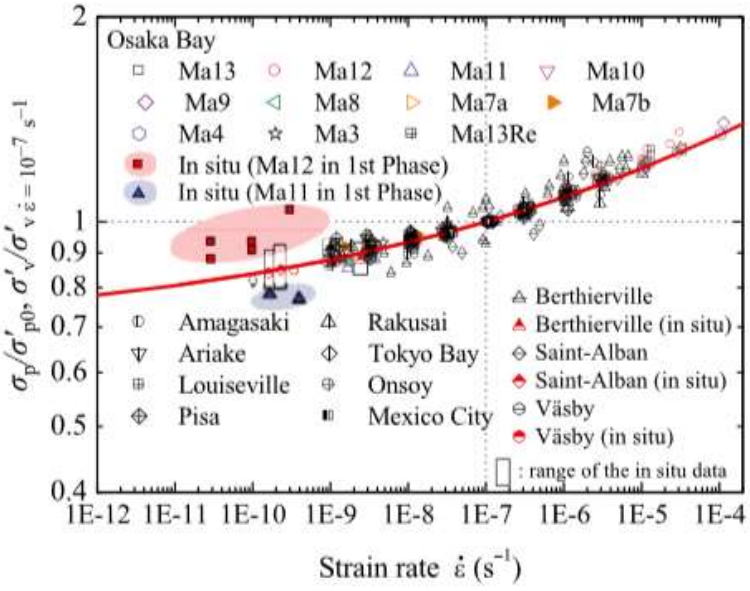

Figure 2-11. The $\log\left(\sigma'_{vy}/\sigma'_{vy,0}\right)$ - $\log\dot{\varepsilon}_{vp}$ *relationship for worldwide clays compared with the intergrated fitting, curve obtained by Eq.* (0.13) *with* $\sigma'_{vy,L}/\sigma'_{vy,0}$ *=0.7,* c_1*=0.935 and* c_2*=0.107 (from: Watabe and Leroueil 2015).*

Leroueil (2006) explains the practical implications of the yield stress dependency on strain rate. Figure 2-12 shows some typical strain rates observed in laboratory testing and in situ. It is shown that the in situ strain rates are significantly smaller than observed in laboratory testing.

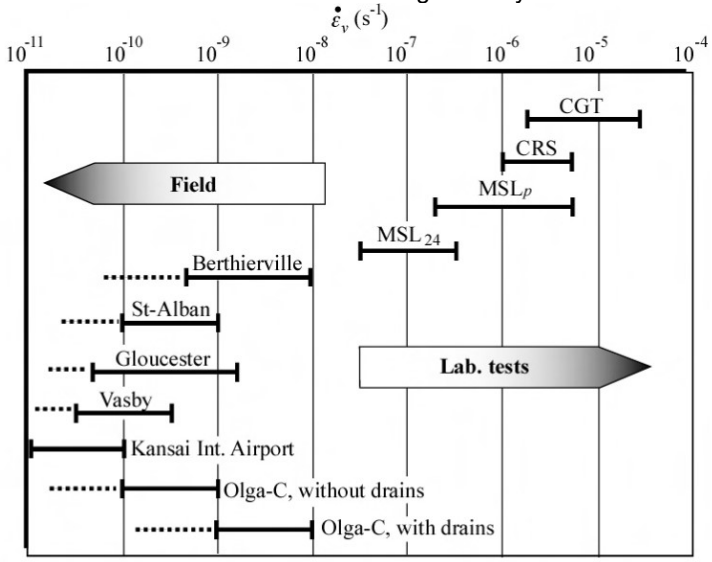

Figure 2-12, Difference in strain rate observed in laboratory testing and in situ, MSL_{24} *= conventional 24h incremental loading oedometer test,* MSL_p *= oedometer test with loading at end of primary, CRS = constant rate of strain tests, CGT = controlled gradient tests, from: Leroueil (2006)*

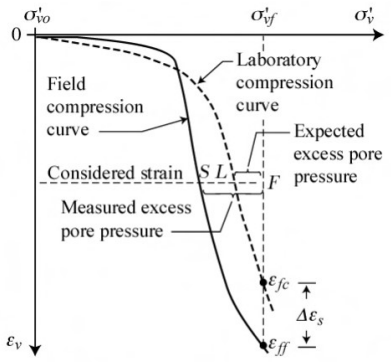

Figure 2-13, Typical compression curve in situ and in laboratory testing, from: Leroueil (2006).

The differences in strain rate should be accounted for in settlement for field conditions, see Figure 2-13. In addition, the authors proposed equations to predict settlement due to creep that will occur in the field in addition to the creep settlement obtained from laboratory tests. In engineering practice settlement behaviour is generally estimated based on the $e-\log\sigma'_v$ curve obtained from a 24-h incremental loading oedometer test, which corresponds to a strain rate of about $1.0\text{x}10^{-7}$ s^{-1}, see point D in Figure 2-14. The additional strain, creep strain corresponding to a strain smaller than $1.0\text{x}10^{-7}$ s^{-1}, in the field , represented by point F in Figure 2-14, can be calculated as a function of $C_c/(1+e_0)$ and in situ strain rate as follows:

$$\Delta\varepsilon_{Field} = \Delta\varepsilon_{D\to F} = \frac{C_C}{1+e_0}\cdot\log\left\{\frac{\sigma'_{p0}}{\sigma'_{pL}}\cdot\left[\frac{1}{1+\exp(c_1+c_2\ln\dot{\varepsilon}_{Field}}\right]\right\} \qquad (0.14)$$

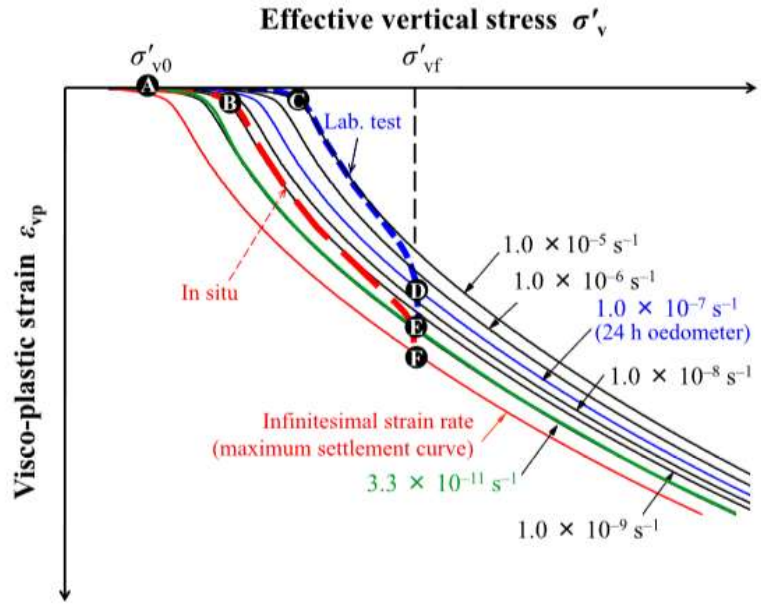

Figure 2-14. Schematic illustration of compression paths for oedometer tests in the laboratory and field behaviour (after: Watabe and Leroueil, 2015)

Eq.(0.14) is charted in Figure 2-15.

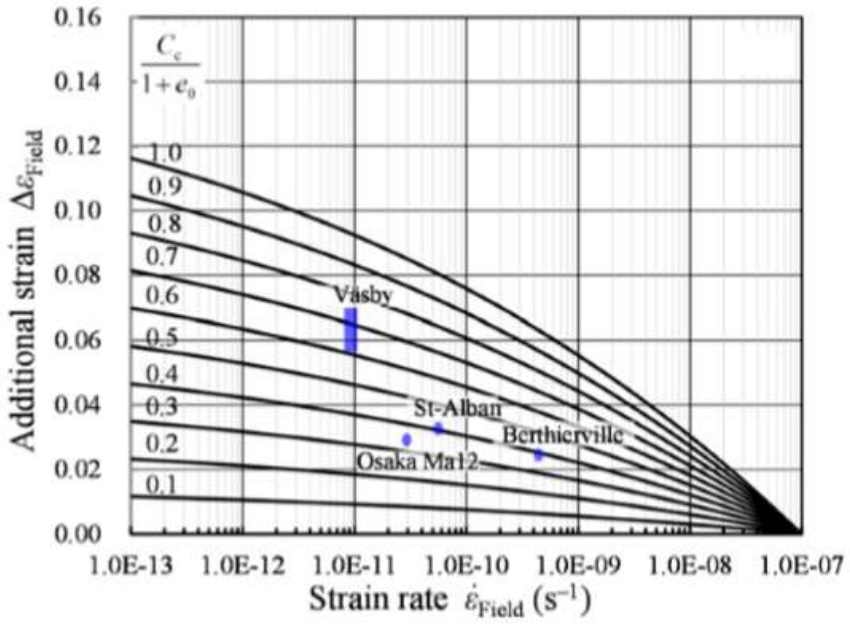

Figure 2-15. Additional strains in the field calculated as a function of Cc/1+e$_0$ and in situ strain rate (after: Watabe and Leroueil, 2015).

By accepting the presence of an infinitesimal strain rate ($\dot{\varepsilon} = 0$) the maximum additional creep strain experienced in the field is given by:

$$\Delta\varepsilon_{ult} = \Delta\varepsilon_{D\to F} = \frac{C_C}{1+e_0}\cdot\log\frac{\sigma'_{p0}}{\sigma'_{pL}} \tag{0.15}$$

This working procedure is summarized by Figure 2-16. A constant rate of strain, CRS, test is used to derive the normalized, reference compression curve. A long-term consolidation test, LT, is used to derive the strain rate development. The authors do not explain how yield stresses are derived. The authors do acknowledge the difficulty in acquiring the soil behaviour at low strain rates. With strain rates in the laboratory typically between 5 × 10^{-8} and 5 × 10^{-5} 1/s the ratio of Cα/Cc, α in Figure 2-9, Figure 2-11, and last graph in Figure 2-16, corresponds well to the values presented by Mesri et al (1995). The deviation of α from a constant Cα/Cc manifest itself more clearly at lower strain rates.

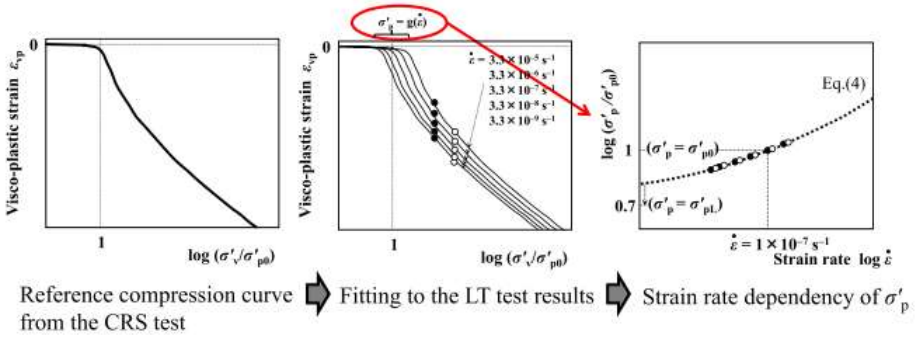

Figure 2-16, Illustration of the method to evaluate the strain rate dependency of yield stress σ'$_{vy}$ from CRS and LT test rests, (from: Watabe & Leroueil, 2015).

2.3.2 Introduction of the concept of zero strain rate isotach

The strain rate dependency of the yield stress, as discussed in section 2.3.1, implies that there is an end to creep, a.o. Leroueil (2006), Watabe & Leroueil (2015). A condition which is represented by the zero strain rate isotach, found for $\sigma'_{vy} = \sigma'_{vy,L}$ in equation (0.13).

Kawabe & Tatsuoka (2013) and others, provide a further exploration of the zero-strain rate isotach. Figure 2-17 shows the field of isotachs including a zero-strain rate isotach. Starting from the refence isotach, the mutual distance between the isotachs decreases for lower strain rates until the zero-strain rate isotach is reached.

There are basically two ways to reach the zero-strain rate isotach, as shown by Figure 2-17. The first is by development of creep strain, the red, vertical, line in Figure 2-17. The second is by unloading, the blue, horizontal, line in Figure 2-17. Is should be noted that reaching the limit isotach in laboratory testing by following the red, vertical, line in Figure 2-17 requires long duration times of the tests and accurate measurements.

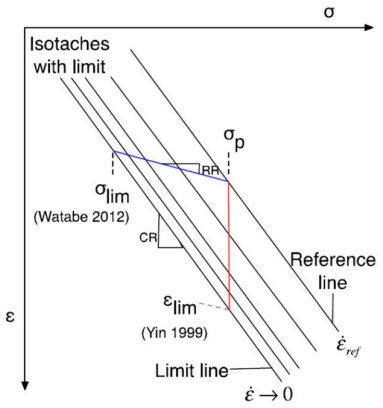

Figure 2-17, Isotachs with creep strain limit, from: Yuan & Whittle (2014)

Kawabe & Tatsuoka (2013) use unloading – reloading loops to establish the isotachs representing low strain rates. The basic rational behind their way of thinking is represented by Figuur 2-18. The strain and corresponding strain rates between the points B and C resemble strain and strain rates between the points B' and C'. Unloading from A to B brings the soil conditions directly at the start of BC, while sustained loading until B' is reached might require considerable testing time and might not be feasible.

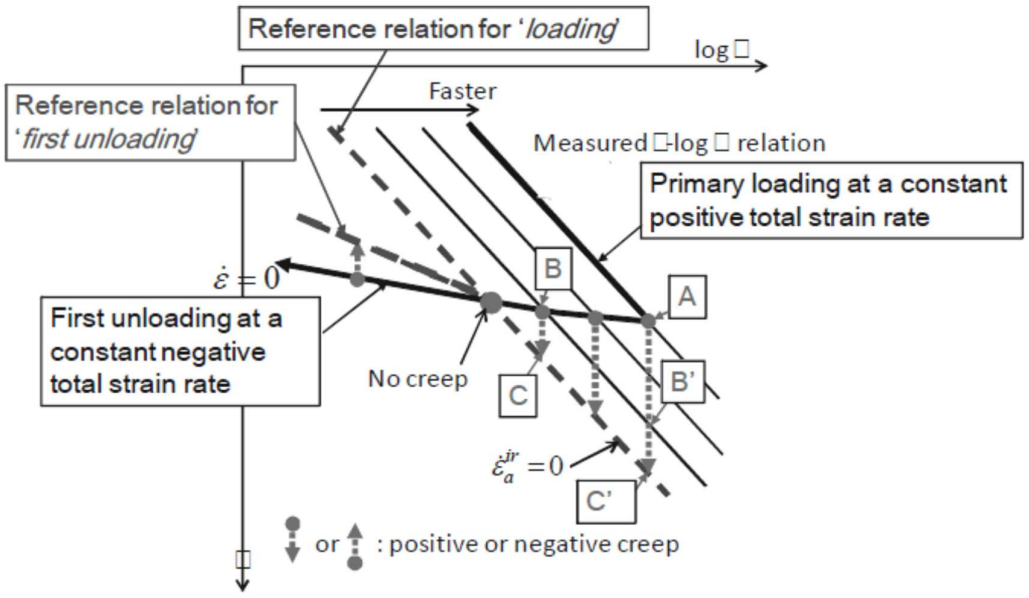

Figuur 2-18, Definition of positive and negative creep, from: Kawabe & Tatsuoka, 2013

In theory, starting from point A in Figuur 2-18 unloading could be applied such that soil conditions reach the limit isotach and no creep develops. Kawabe & Tatsuoka (2013) intoroduce positive and negative creep. When soil is unloaded beyond the limit isotach negative creep develops representing a volume increase or a swelling of the ground level. In contrast, the positive creep represents a volume reduction or settlement of the ground level.

Figuur 2-18 defines two limit isotachs referred to as reference relation in Figuur 2-18. As long as creep strain rates remain positive the limit isotach is represented by the reference relation for loading. When exceeding the reference relation for loading, for example due to unloading, negative creep strain and corresponding negative creep strain rates develop until the reference relation for first unloading is reached.

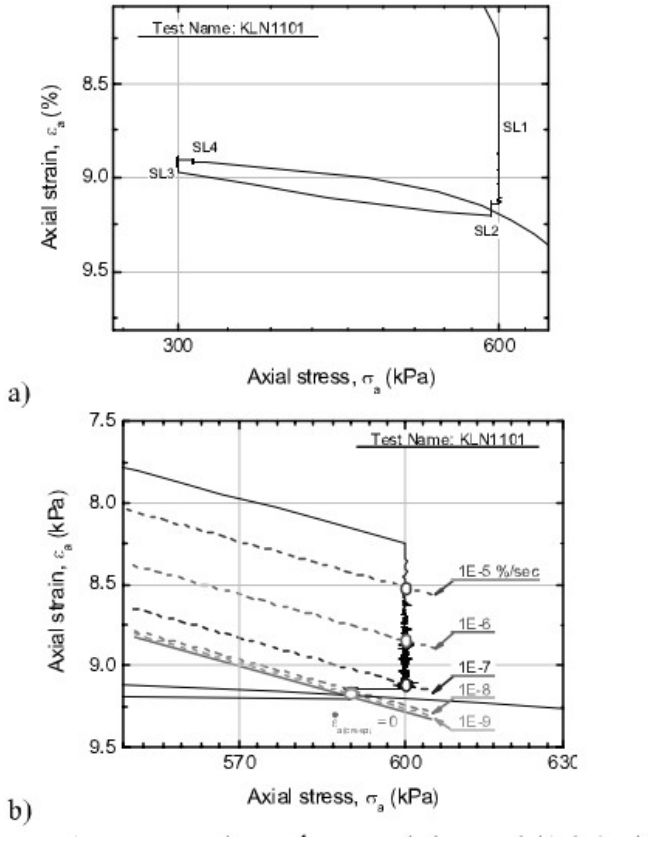

Figure 2-19, Creep rate development during a load cycle including phases of sustained loading, SL after: Kawabe & Tatsuoka, 2013

Figure 2-19 shows measurement data of an oedometer test on Fujinomori clay. The test includes loading until an axial stress of 600 kPa followed by sustained loading, SL1, a small unloading followed by sustained loading, SL2, large unloading until an axial strain of 300 kPa followed by sustained loading, SL3, a small reloading in combination to sustained loading, SL4 and finally large reloading. Figure 2-19a shows the stress strain curve. Figure 2-19b zooms in and shows the developed strain rates and corresponding isotachs by the dotted lines. The limit isotach or reference relation for loading is indicated by a continuous line. The graph shows a reduction in strain rate for the lower isotachs and a reduction in mutual distance between the isotachs. It is remarkable that the distance between the isotachs with a strain rate up to 1×10^{-7} 1/s are clearly larger than found for the isotachs with lower strain rates. Kawabe & Tatsuoka (2013) conclude: “The logarithm of creep strain rate decreases rather linearly with creep strain until the creep strain rate becomes a certain low value, followed by a drastic decrease toward zero”.

It should be noted that the strain rates up to 1×10^{-7} 1/s follow from the first sustained loading phase, SL1, while the lower strain rates follow from SL2, SL3 and SL4.

Zwanenburg (2017) discusses a series of CRS tests conducted to test the limit isotach concept for peats. The tests contained unloading followed by relaxation under constant height. The rational behind application of the relaxation phase in CRS testing follows from swelling that would occur after unloading in conventional oedometer tests. The swelling will consist of elastic part due to the load reduction and visco-plastic behaviour. To avoid the problems in dividing the measured swell in an elastic and visco-plastic part, relaxation was applied rather than unloading. The vertical stress development during the relaxation phase

reflects the nature of the creep as discussed by Figuur 2-18. A reduction in vertical stress reflects a tendency for volume reduction and therefore positive creep, while a vertical stress increase reflects a tendency for volume increase and negative creep.

Figure 2-20 shows the results of 5 tests. The level of unloading is reflected in the presented OCR. For increasing OCR the effect of swell becomes more pronounced, however after reaching a peak, the vertical stress declines again indicating a volume reduction and therefore positive creep. In these tests no indication of a limit isotach was found for peats.

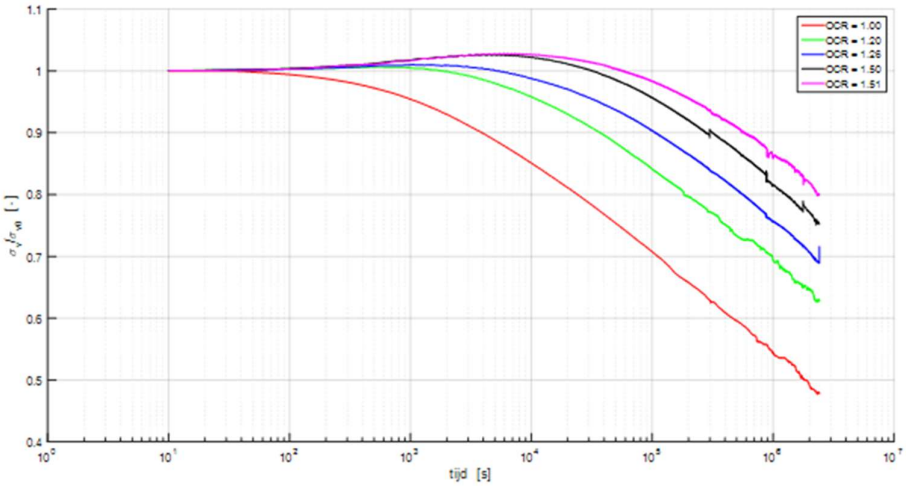

Figure 2-20, Development of vertical stress during a relaxation phase after unloading for different levels of unloading, from: Zwanenburg (2017)

It should be noted that the outcome of Figure 2-20 seems to correspond to Samson (1985). Figure 2-21 shows measurements of the top of an embankment build on a peat foundation, using pre-loading. Removal of the pre-loading induces an immediate rebound followed by swell and finally settlement.

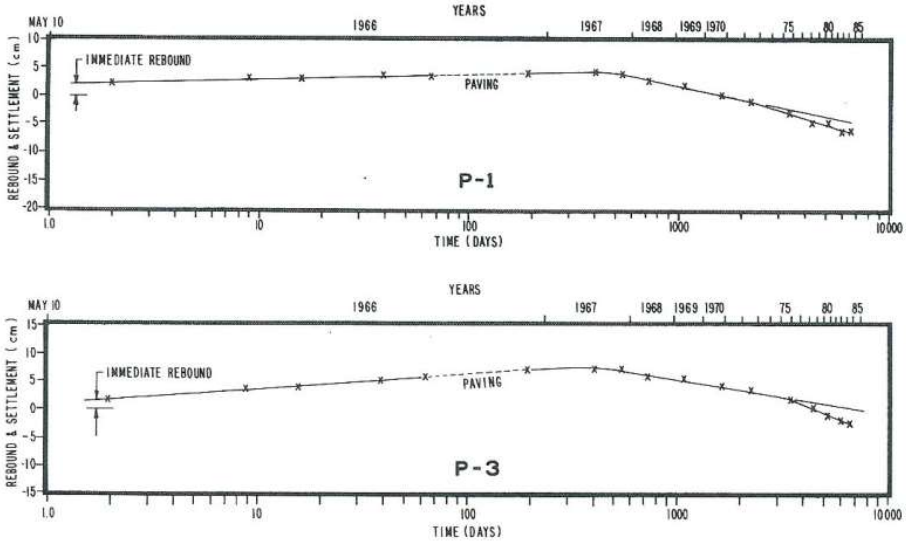

Figure 2-21, Rebound, swell and settlement of road construction using pre-loading, from: Samson (1985)

2.3.3 Introduction of an internal state variable for assessing the viscoplastic strain rate, MIT-SR model

Yuan and Whittle (2016) proposed an elasto-viscoplastic formulation for assessing the compression behaviour of clays in which the viscoplastic strain rate is attributed to an internal state variable. This variable represents the perturbation of clay particles due to the prior strain history**.** According to the authors, this formulation overcomes two basic drawbacks of existing isotach models. That is:

(i) Based on the existing isotach model the viscoplastic strain rate is uniquely defined by the state of vertical stress and void ratio. However, in the isotach model the adoption of a reference creep rate as obtained at laboratory scale will likely lead to an overestimation of the creep settlements at the end of primary consolidation. This is because the actual strain rate experienced in the field will be lower than the reference strain rate for the same vertical stress and void ratio applied in the laboratory. The overestimation of settlement due to creep is enhanced as the thickness of the clay layer encountered in the field increases and the time required to reach the end of primary consolidation increases. In the elasto-viscoplastic formulation proposed by Yuan and Whittle (2016) the viscoplastic strain rate is not considered as a function of the vertical stress and void ratio but a function of an internal strain rate.

(ii) Ladd et al. (1977) frames the hypothesis A and B concepts when it comes to typical observations in settlement behaviour. The isotach model conforms to a Hypothesis B behaviour. Although it is well demonstrated in the literature that the measured time – dependent compressibility of clays agrees very well with creep Hypothesis B behaviour (Degago et al., 2011) there are still laboratory and field data that support both Hypothesis A and B (Mesri, 2009; Choi, 1982). The newly introduced elasto-viscoplastic formulation by Yuan and Whittle (2016) is capable of simulating both hypothesis A and B.

In the proposed formulation, an internal strain variable, R_a (≥0), is introduced and the visco-plastic strain rate, $\dot{\varepsilon}_{vp}$, is calculated as follows:

$$\dot{\varepsilon}_{vp} = R_a \cdot \left(\frac{\sigma'_v}{\sigma'_p}\right) \tag{0.16}$$

Where:

σ'_v = the vertical effective stress

σ'_p = reference stress state defined in the $\log e - \log \sigma'_v$ space.

The internal strain rate $\dot{R}_a$ can be calculated considering a function of the total strain rate, $f(\dot{\varepsilon})$ and a transient coefficient, m_t :

$$\dot{R}_a = \left[f(\dot{\varepsilon}) - R_a \right] \cdot m_t \tag{0.17}$$

A schematic illustration of Eq. (0.17) is given by Figure 2-22 which shows the evolution of R_a during CRS compression and relaxation.

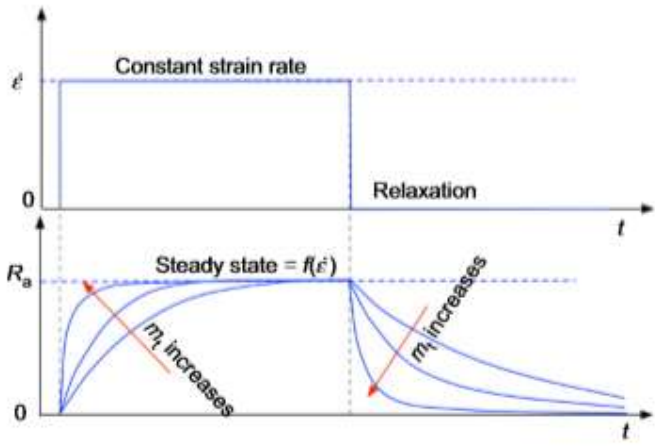

Figure 2-22. Influence of m_t on the evolution of R_a during CRS compression and relaxation (after: Yuan and Whittle, 2018).

The R_a converges to a steady state condition which is a function of the applied strain rate, $f(\dot{\varepsilon})$. At the steady state condition $\dot{R}_a$ in Eq. (0.17) is 0, and $f(\dot{\varepsilon}) = R_a$. The $f(\dot{\varepsilon})$ is defined for matching the normal consolidation characteristics in CRS tests. Consequently,

$$f(\dot{\varepsilon}) = R_a = \left(\frac{\rho_c - \rho_r}{\rho_c}\right) \cdot \dot{\varepsilon} \cdot \left(\frac{\dot{\varepsilon}}{\dot{\varepsilon}_{ref}}\right)^{-\beta} \tag{0.18}$$

And Eq. (0.16) becomes:

$$\dot{\varepsilon}_{vp} = \left(\frac{\rho_c - \rho_r}{\rho_c}\right) \cdot \dot{\varepsilon} \cdot \left(\frac{\dot{\varepsilon}}{\dot{\varepsilon}_{ref}}\right)^{-\beta} \cdot \left(\frac{\sigma'_v}{\sigma'_p}\right) \tag{0.19}$$

Where,

ρ_c = compression ratio;

ρ_r = recompression ratio;

β = rate dependent parameter of steady state of R_a;

ρ_a = creep coefficient

$\dot{\varepsilon}_{ref}$ = reference strain rate.

The transient coefficient m_t is assumed to be a function of the visco-plastic strain rate:

$$m_t = \left(\frac{\rho_c}{\rho_a} - 1\right) \cdot \frac{\dot{\varepsilon}_{vp}}{\rho_r \cdot n} + \dot{\varepsilon}) \tag{0.20}$$

As can be seen in the equations above, the proposed model has five material constants (ρ_c, ρ_r, ρ_a β , $\dot{\varepsilon}_{ref}$) and two internal state variables (σ'_p, R_a). The material constants and the state variable σ'_p can be experimentally determined from CRS and IL oedometer tests. For

overconsolidated state [σ'_p/σ'_v>2], the authors propose an intial R_{a0} = 0 (negligible creep).

For normally consolidated clay the initial creep rate $\dot{\varepsilon}_{vp,0} \sim R_{a0}$, see Eq. (0.16) for σ'_p/σ'_v =1.

The initial creep rate can be calculated by knowing the thickness of the clay layer in the field, the creep coefficient and the soil porosity and by assuming that a degree of consolidation of 99% is achieved.

The parameter β in Eq. (0.19), describing the rate-dependency of the steady state behaviour, has a constant value irrespective of strain rate. The parameter β value is physically bounded such that $0 \leq \beta \leq \frac{\rho_a}{\rho_c}$. For $\beta = \frac{\rho_a}{\rho_c}$, Eq. (0.19) is in agreement with the conventional isotach formulation, which includes parallel compression lines in the void ratio – log σ_v' space with each corresponding to a specific strain rate. For β =0, a unique compression curve is obtained independent of the applied strain rates, hypothesis A behaviour. In Figure 2-23, the creep curve as predicted based on the proposed model for different β values is shown for the case of a clay sample in a CRS test.

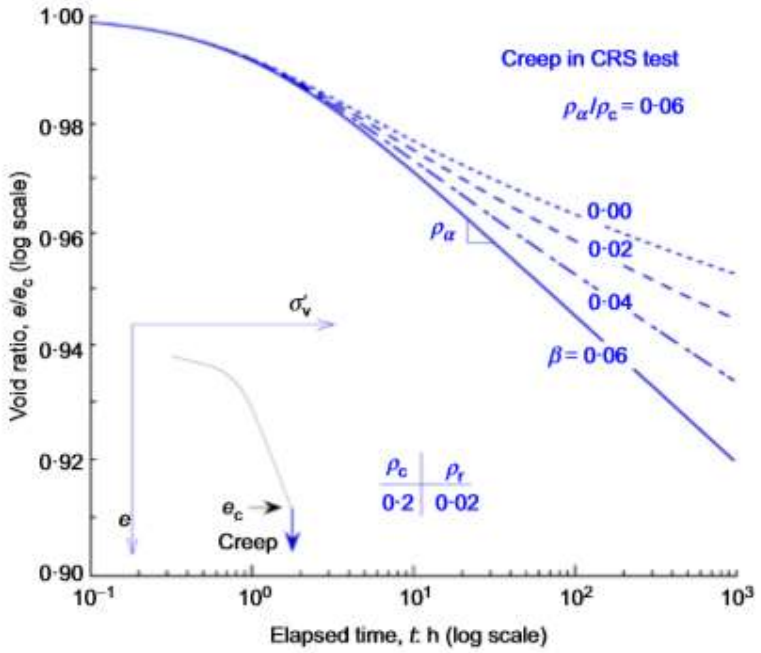

Figure 2-23. Creep for different values of β (after Yuan and Whittle, 2018).

2.3.4 Introduction of an OCR dependent secondary compression index

In most of the existing isotach models, it is assumed that the isotachs are equally spaced in terms of ratios of strain rates while the slope of each isotach in the effective stress - strain space is constant. This implies a constant value for the secondary compression coefficient, $C_{\alpha\varepsilon}$. Yuan et al. (2015), however, have shown that the creep behaviour for soils that are unloaded to moderate overconsolidation ratios can be predicted based on a modified isotach formulation in which the secondary compression coefficient varies with OCR. Specifically, the development of creep strain, ε, under constant stress is expressed by a simple two parameter model as follows:

$$\varepsilon = 0.434 \cdot \hat{C}_{\alpha\varepsilon} \cdot \ln\left(\frac{\dot{\varepsilon}_1}{\dot{\varepsilon}}\right) \tag{0.21}$$

The material input parameters $\hat{C}_{\alpha\varepsilon}$ and $\dot{\varepsilon}_1$ in the above equation depend on the stress history of the clay (OCR) and they were determined experimentally based on a data-fitting approach of oedometer tests on natural clay samples. For an induced OCR of less than 1.5, $\hat{C}_{\alpha\varepsilon}$ and $\dot{\varepsilon}_1$ are given by:

$$\frac{\hat{C}_{\alpha\varepsilon}}{C_{\alpha\varepsilon}} = \frac{2}{OCR^{\beta}+1} \tag{0.22}$$

$$\frac{\dot{\varepsilon}_1}{\dot{\varepsilon}_r} = \left(\frac{1}{OCR}\right)^{m} \tag{0.23}$$

Where:

- $C_{\alpha\varepsilon}$ = the secondary compression coefficient of the normally consolidated clay samples. For OCR=1, $\hat{C}_{\alpha\varepsilon}$ = $C_{\alpha\varepsilon}$ (conventional isotach model).
- β = parameter that controls the rate of decrease of $\hat{C}_{\alpha\varepsilon}$ / $C_{\alpha\varepsilon}$ with OCR
- $\dot{\varepsilon}_1$ = the creep rate immediately after unloading and
- $\dot{\varepsilon}_r$ = the strain rate before removal of surcharge.

Based on Eq. (0.21), (0.22) and (0.23) it can be concluded that the conventional isotach model ($\hat{C}_{\alpha\varepsilon}$ = $C_{\alpha\varepsilon}$) overestimates the post-unloading creep strains. For instance, for OCR=1.5 and a β = 7.2, as determined for the clay samples in the study of Yuan et al. (2015), Eq. (0.22) predicts a $\hat{C}_{\alpha\varepsilon}$ that is approximately 10% of the $C_{\alpha\varepsilon}$ value.

2.3.5 Introduction of distorted isotachs, C+S model

Den Haan & Edil (1994) noticed that after unloading – reloading of Wisconsin peat creep strain rate remains larger than would be predicted by the reference implementation used in this report, section 2.2.1. The observation is explained by structural changes due to unloading reloading. This phenomenon is further explored by Nash (2010) and Nash & Brown (2015). Figure 2-24, taken from Nash & Brown (2015), shows the distortion of the isotachs by the dotted lines. The curvature is explained by the destructuration of soil upon reloading. Nash (2010) modified the model by Claesson (2003) to include the curvature of the isotachs around the yield stress as follows:

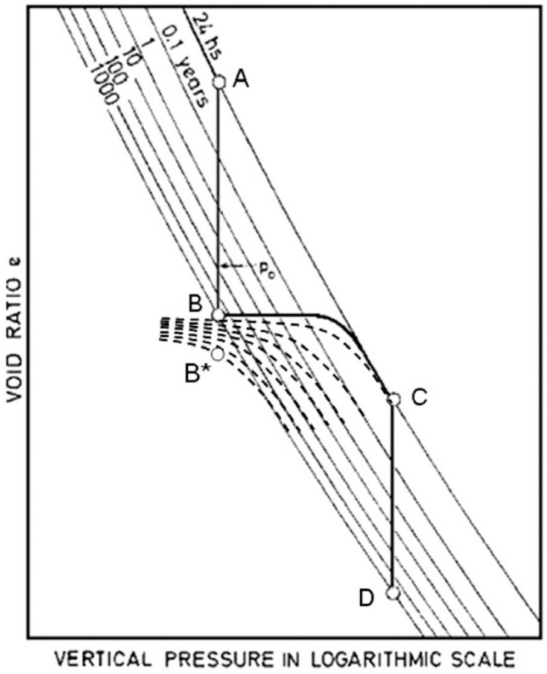

Figure 2-24 Distorted isotachs in overconsolidated region, from: Nash & Brown (2015)

The creep strain and creep strain rate are given by:

$$\Delta\varepsilon^c = \frac{\psi}{v_0}\ln\left(1+\frac{t_e}{t_0}\right); \quad \dot{\varepsilon}^c = \frac{\psi}{v_0\left(t_0+t_e\right)}; \quad \dot{\varepsilon}_0^c = \frac{\psi}{v_0 t_0} \tag{0.24}$$

In which:

ψ = creep parameter, $\psi = C_\alpha / \ln(10)$
v_0 = initial specific volume
t_0 = reference time
t_e = equivalent time
$\dot{\varepsilon}^c$ = reference creep strain rate

Equation (0.24) is used to evaluate creep strain for normally consolidated conditions. The curvature in over consolidated conditions is found by a reduction in ψ, according to:

$$\psi = \beta\psi_{NC} \tag{0.25}$$

In which:

ψ_{NC} = creep parameter for normally consolidated conditions
β = reduction factor

The reduction factor, β, is expressed as a sine-function. To bound the reduction factor to the overconsolidated region β is linked to the time resistance parameter and time resistance number as used in the Swedish practice and illustrated by Figure 2-25 (Nash & Brown, 2015;Claesson, 2003).

$$\beta = \beta_{\min} + \left(1-\beta_{\min}\right)\sin^a\left(\eta\right), \quad \eta = \frac{\pi}{2}\frac{b-b_0}{b_1-b_0} \tag{0.26}$$

In which:

β_{min} = minimal value, input parameter

a = power

b = ratio of actual effective stress over yield stress, $b = \sigma' / \sigma_y$

b_0, b_1 = stress ratio's see Figure 2-25c

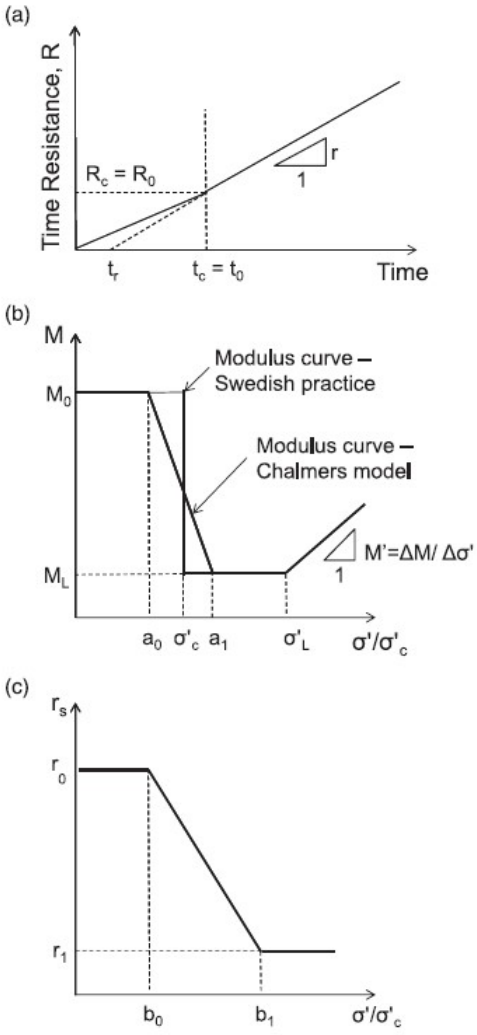

Figure 2-25 Principle sketch of time resistance parameter, R, constrained modulus, M and time resistance factor r as a function of the stress ratio, σ'/σ'_c from: Nash & Brown (2015). R = dt/dε and $\sigma'_c = \sigma_y$

The time resistance parameter, *R* is the inverse of the strain rate *R* = d*t*/dε. The time gradient, *r* of *R* changes in the region of the yield stress, as shown by Figure 2-25c. Equation (0.26) allows β to change from its minimal value to 1 when *b* = b_1. The parameters β_{min} and *a* follow from fitting laboratory test data.

Nash & Brown (2015) explain the curvature of the isotachs by destructuration upon reloading and suggest using the distortion of the isotachs for any overconsolidated conditions independent whether the overconsolidation was reached by aging or unloading. This conclusion follows from a qualitative comparison to field experience and a comparison of calculation result found by different models that account and do not account for destructuration.

In contrast Vergote (Vergote, 2020, Vergote et al., 2020, 2021) explains the distortion of the isotachs by swelling during unloading and proposes a model which includes swelling after unloading. This model is referred to as the Creep and Swell model, C + S model.

The key notion of the C + S model is that swelling is transient process, which, in contrast to creep, is not modelled by isotach-behaviour.

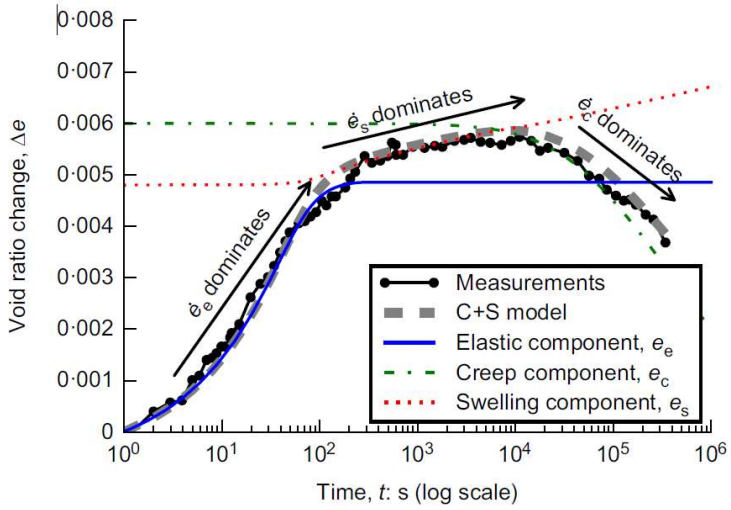

Figure 2-26, Principle of the C+S model: decomposition of strain rates in an elastic, swelling and creep rate component. From: Vergote et al. (2020).

Figure 2-26 shows how, according to the C + S model, volume change after unloading is followed by an elastic component, a swelling component and creep.

The decoupling of swell and creep in the C+S model results in the use of two definitions for the overconsolidation ratio. Creep rate is related to position of the current stress state in relation to the reference isotach. This position is defined by the yield stress, $\sigma'_{p.ref}$, which is a position on the reference isotach and changes in time due to aging. The swelling rate depends on the level of unloading related to the ratio of the maximum stress before unloading and the actual stress;

$$OCR = \frac{\max(\sigma')}{\sigma'}, OCR_{ref} = \frac{\sigma'_{ref}}{\sigma'} \tag{0.27}$$

The strain rate in the C+S model is a summation of three components, the elastic strain rate, $\dot{e}_e$, the compressive viscoplastic strain rate, $\dot{e}_{vp,c}$ and swelling rate, $\dot{e}_s$:

$$\dot{e} = \dot{e}_e + \dot{e}_{vp,c} + \dot{e}_s \tag{0.28}$$

It should be noted that the swelling strain rate is positive for a volume increase while the elastic and the compressive viscoplastic strain rates are positive for a volume reduction.

The elastic strain rate follows from the loading rate:

$$\dot{e}_e = C_r \frac{\dot{\sigma}'}{\sigma'} \frac{1}{\ln(10)} \tag{0.29}$$

In which:

C_r = re-loading compression index

$\dot{\sigma}'$ = loading rate

The compressive viscoplastic strain rate follows from the initial strain rate directly after loading, $\dot{e}_{init,c}$ and the update of the creep parameter $\hat{C}_{\alpha,c}$:

$$\frac{\dot{e}_{init,c}}{\dot{e}_{vp,c,ref}} = \left(\frac{1}{OCR}\right)^{\beta_3} \tag{0.30}$$

In which:

$\dot{e}_{init,c}$ = Creep rate directly after unloading

$\dot{e}_{vp,c,ref}$ = creep strain rate on the reference isotach

β_3 = control parameter creep strain rates

For $\beta_3 = (C_c - C_r)/C_\alpha$, equation (0.30) represents the condition of a linear isotach model with equally spaces isotachs. The distortion of the isotachs is found from an update of the creep parameter $\hat{C}_{\alpha,c}$:

$$\frac{\hat{C}_{\alpha,c}}{C_{\alpha,ref}} = \frac{2}{\left(\dot{e}_{vp,c} \,/\, \dot{e}_{vp,c,ref}\right)^{-\beta_2/\beta_3} + 1} \tag{0.31}$$

In which:

β_2 = control parameter decay C_α, see equation

The C+S models allows for both equidistance isotachs and non-equidistance isotachs. For non-equidistance isotachs the creep parameter C_α declines, see also section 2.3.4. In the C+S model the change in C_α follows from:

$$\frac{\hat{C}_{\alpha}}{C_{\alpha,ref}} = \frac{2}{OCR_{ref}^{\beta_2} + 1} \tag{0.32}$$

In which:

$C_{\alpha,ref}$ = creep parameter C_α at reference isotach

The swelling rate follows from:

$$\dot{e}_{initial,s} = 10^{b_2}\left(OCR_{ref} - 1\right)^{m_2} \tag{0.33}$$

$$\ddot{e}_s = -\frac{1}{\hat{C}_{\alpha,s}}\dot{e}_s^2 \ln(10) + m_2 \frac{\dot{OCR}}{OCR - 1} \tag{0.34}$$

$$\frac{\hat{C}_{\alpha,s}}{C_{\alpha,ref}} = 10^{b_1}\left(OCR - 1\right)^{m_1} \tag{0.35}$$

In which:

$\dot{e}_{initial,s}$ = initial swelling rate, directly after unloading

b_2, m_2 = parameters controlling the change in initial swelling rate

$\hat{C}_{\alpha,ref}$ = swelling parameter

b_1, m_1 = parameters controlling the swelling parameter

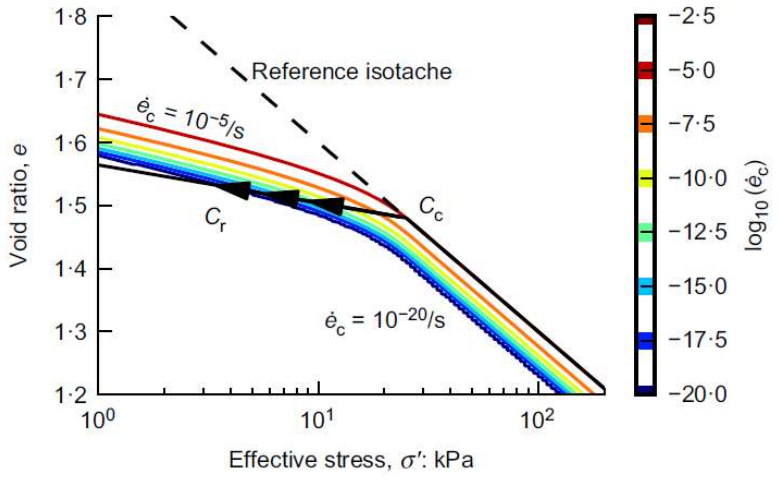

Figure 2-27, Example of distorted creep isotachs based on β_2 = 4 and β_3 = 19, from: Vergote et al. 2020

Figure 2-27 shows an example of the field of distorted isotachs taken from Vergote et al. (2020).

The C+S model uses 10 parameters of which four are typically derived from conventional incremental loading or constant rate of strain tests, The remaining parameters can be evaluated from curve fitting and parameter optimization, as shown by Vergote et al (2020) and (2021).

3 Discussion on Literature study

3.1 Exploring the MIT-SR model

Section 2.3.3 discusses the MIT-SR model presented by Yuan & Whittle (2018). This section provides a further exploration of this model and studies the influence of the different parameters. To facilitate the exploration of the model spreadsheet implementations were built. The implementations contain a direct implementation, which gives changes in void ratio as a function of stress increment, which was used to study creep under constant loading. An inverse implementation was built, which provides stress as function of void ratio, to model constant rate of strain tests.

Table 3-1 provides the applied soil parameters. To test the implementations, Figure 3-1 and Figure 3-2 are created to reproduce Fig. 3a and 3b from Yuan & Whittle (2018). The graphs are similar, and it is concluded that the implementations work correctly. The simulations reproduce the relevant phenomena; For $\beta = \rho_\alpha / \rho_c$, Figure 3-1, the model behaves like a conventional isotach model. For $\beta = 0$, Figure 3-2, all isotachs fall together and a strain rate increase results in a temporarily deviation from the compression line. It should be noted that if β is increased to a large value; $\beta = 0.5$, the isotachs remain parallel, see Figure 3-3. It seems that in the model the isotach distance is given by β instead of ρ_α.

Table 3-1, Applied soil parameters

parameter	unit	value
ρ_r	[-]	0.02
ρ_c	[-]	0.2
ρ_α	[-]	0.012
$d\varepsilon/dt_{ref}$	[1/uur]	0.005
σ'_{vy}	[kPa]	10
β	[-]	0.067

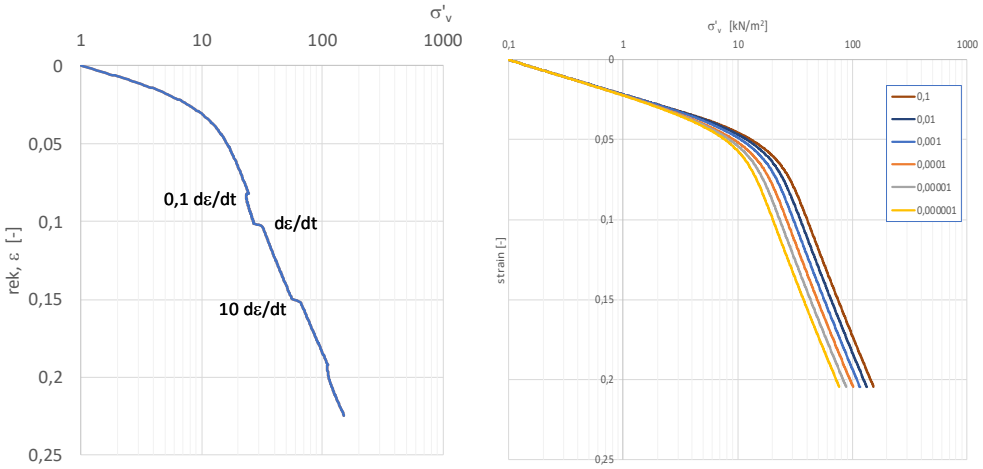

Figure 3-1, Simulations of Yuan & Whittle model, parameters are given in Table 3-1, reproduction of Fig. 3a, β = 0.06, from Yuan & Whittle, 2018. Left: loading path including changes in loading rate, right: loading paths for loading rates changing from 0.1 to 0.000001 1/s

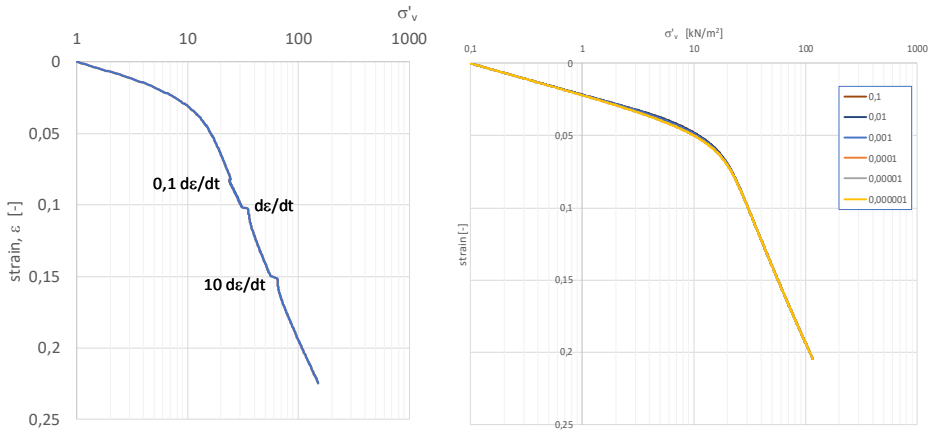

Figure 3-2, Simulations of Yuan & Whittle model, reproduction of Fig. 3b; β = 0 other parameters are given in Table 3-1, from Yuan & Whittle, 2018. Left: loading path including changes in loading rate, right: loading paths for loading rates changing from 0.1 to 0.000001 1/s

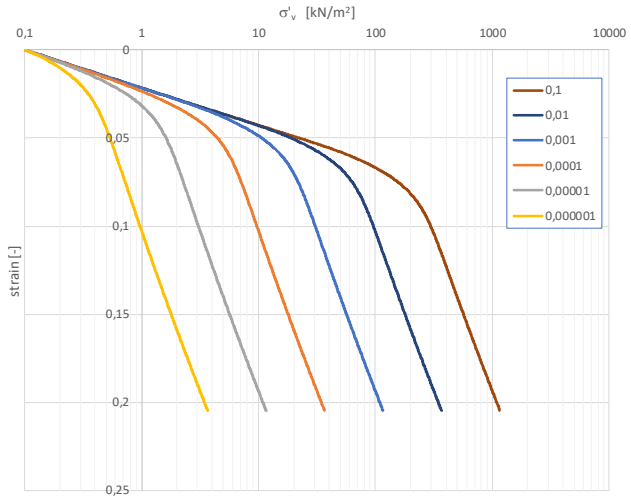

Figure 3-3, Isotach field for β = 0.5. Left: loading path including changes in loading rate, right: loading paths for loading rates changing from 0.1 to 0.000001 1/s

The use of a β-value independent from the compression ratio's allows to model non-linear isotachs. The influence of β on the creep rate and development of OCR due to aging is shown by Figure 3-4 and Figure 3-5.

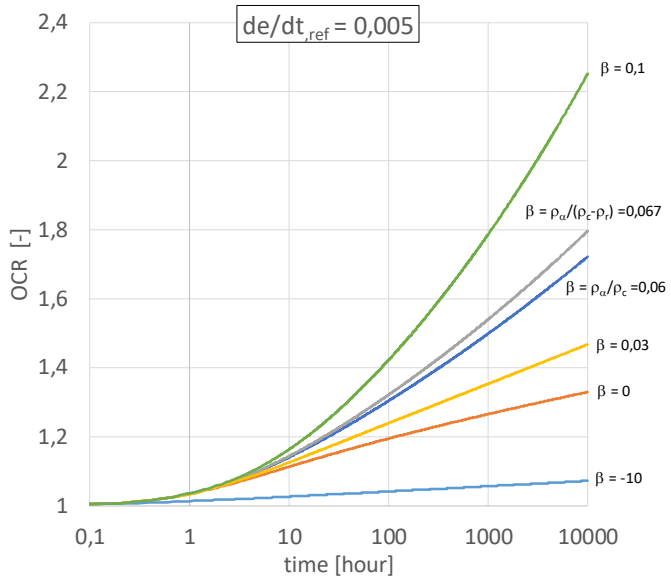

Figure 3-4, Development OCR in time for different β-values

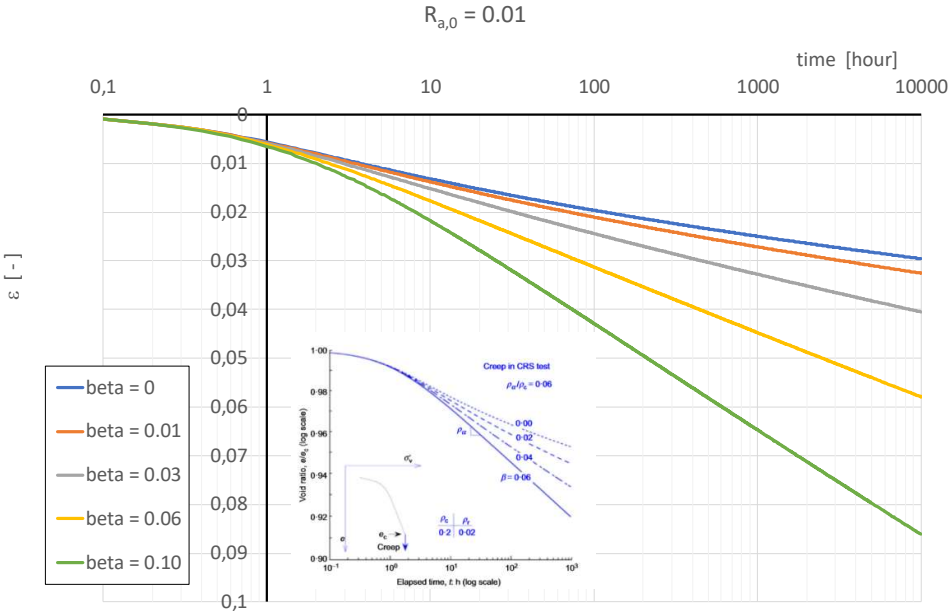

Figure 3-5, Creep strain under constant loading, starting at normally consolidated conditions, for $R_{a,0}$ = 0.01

The internal strain variable R_a controls the development of the creep rate. To illustrate this Figure 3-5 is redrawn by Figure 3-6, for the initial value $R_{a,0}$ = 0 instead of 0.01. A low starting value of R_a causes the strain rate to start at a low level and increase when strain develops.

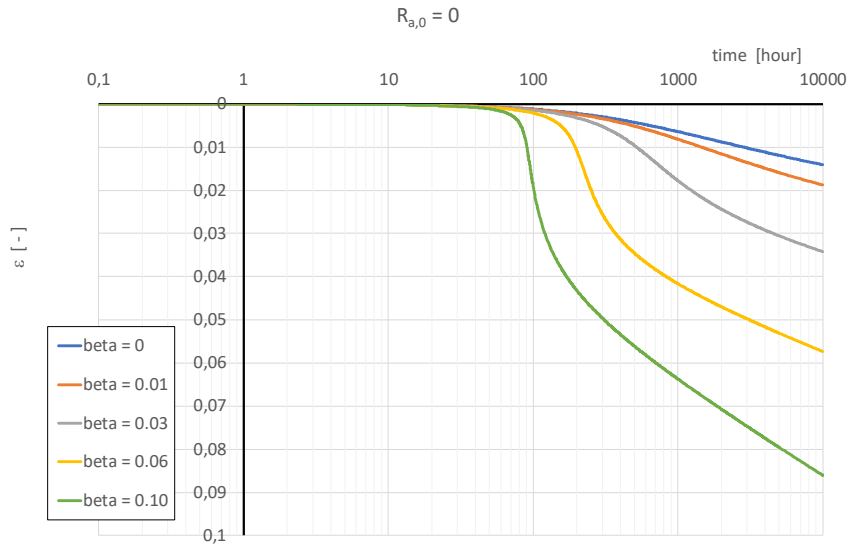

Figure 3-6, Creep strain under constant loading, starting at normally consolidated conditions, for $R_{a,0}$ = 0

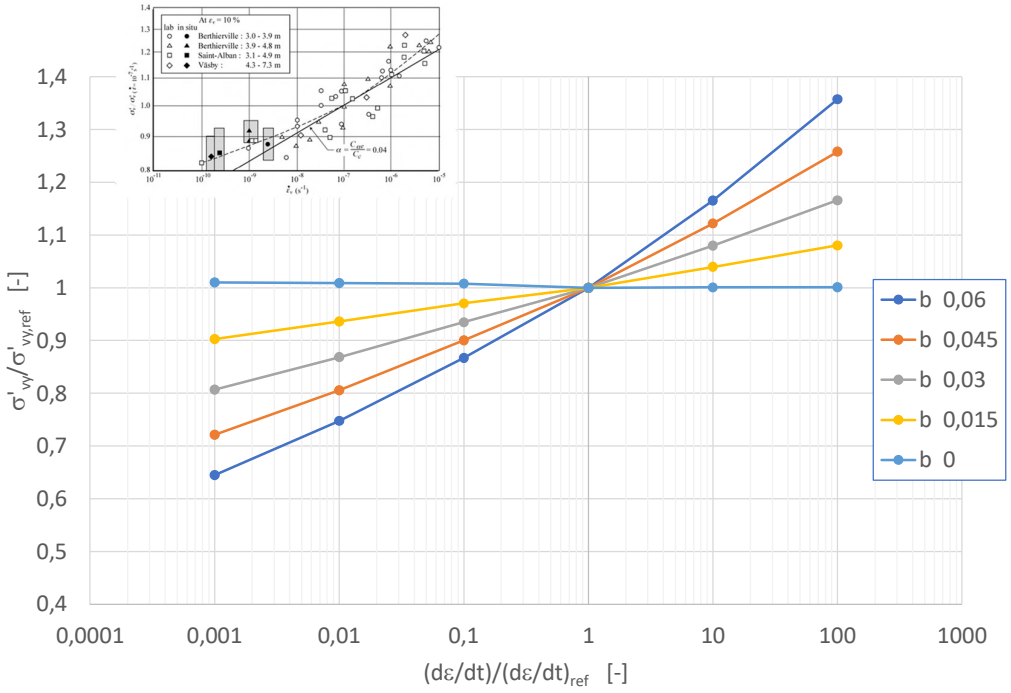

Figure 3-7, Relation between strain rate and yield stress for the MIT-SR model

Section 2.3.1 discusses the relation between the yield stress and strain rate. Figure 3-7 shows the results of series simulation te reproduce Figure 2-9. It should be noted that for β = 0, all isotachs fall together and the line in Figure 3-9 reduces to a horizontal line at $\sigma'_{vy} / \sigma'_{vy,\,ref}$ = 1.0. Due to numerical issues at low strain rates, small deviations are found for β = 0 in Figure 3-9. Figure 2-9 seems to suggest a curved relation between the yield stress and logarithm of the strain rate, the dotted line in Figure 2-9. Except from the reference strain rate, the ratio of $\sigma'_{vy} / \sigma'_{vy,ref}$ for the different strain rates is above the line predicted by linear isotachs. Changing the β-value in the MIT-SR model results in a rotation of the $\sigma'_{vy} / \sigma'_{vy,ref}$ – in strain rate relation. For $\beta < \rho_\alpha / \rho_c$ might better reproduce measurements of the ratio σ'_{vy} /

$\sigma'_{vy,ref}$ for strain rates below the reference strain rate. However, for strain rates above the reference strain rate, $\beta < \rho_\alpha / \rho_c$ underpredicts the trend for $\sigma'_{vy} / \sigma'_{vy,ref}$.

3.2 Exploring the C+S model

Vergote et al. (2020) discuss the consequences of equation (0.28), stating that the creep strain rate follows from the summation of the elastic strain rate, the compressive creep strain rate and swelling strain rate. In this formulation the swelling rate and creep strain rate are not mutually exclusive. As shown by Figure 2-26, upon unloading, after the elastic swelling the compressive creep strain will, typically, dominate the swelling strain after some time. This contrasts with the models discussed by a.o. Kawabe & Tatsuoka (2013), where creep and swelling are mutually exclusive, and a neutral zone can be identified where no creep or swelling occurs.

This represents a significant difference in behaviour. Following Vergote et al. 2020 and 2021, creep following swell is more in alignment with the experimental data, see also Figure 2-20 and Figure 2-21.

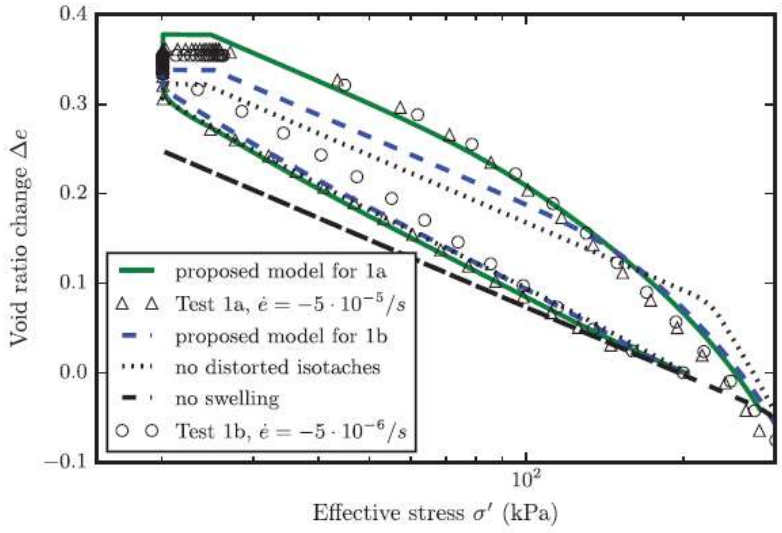

Figure 3-8, example of modelling the unloading – reloading cycle, from: Vergote et al (2021)

The de-coupling of swelling and creep allows the C+S model to model the unloading – reloading hysteresis, see Figure 3-8, from Vergote et al. (2021). For models that do not account for swelling the unloading and reloading line falls together to a single line, the dotted line in Figure 3-8 indicated by no-swelling.

It is interesting to note that in the C+S model, the distortion of the isotachs are coupled to unloading. For conditions in which the load is kept constant for a long time and OCR develops due to aging, the isotachs remain undisturbed and the development of creep strain rates due to (re)loading until the yield stress or beyond is based on the non-distorted isotachs. This seems in contrast to Nash & Brown (2015), where the isotachs in the overconsolidated region are assumed to be distorted independent from the origin of consolidation, unloading or aging.

A further exploration of the C+S model is given by Dick (2022). Simulation of an embankment construction shows that for loading conditions te C+S model can yield the same settlement

prediction as the linear isotach model, discussed in section 2.2.1 depending on the selection of β_2 in equation (0.32). As is to be expected differences occur upon unloading. Figure 3-9 shows an example of settlement prediction of embankment construction, including pre-loading. For details of eth analysis, see Dick (2022). Upon unloading, as expected, the C+S model predicts more swell than the linear isotach model. The C+S model predicts a higher strain rate compared to the isotach model and consequently, for the applied parameterset, the settlement at 30 years are equivalent for the C+S and linear isotach model.

Figure 3-10 shows the differences between the reference implementation, referred to as linear isotachs, and C+S model including non-linear isotachs. For non-linear isotachs less residual settlement is found after unloading then found by the reference model.

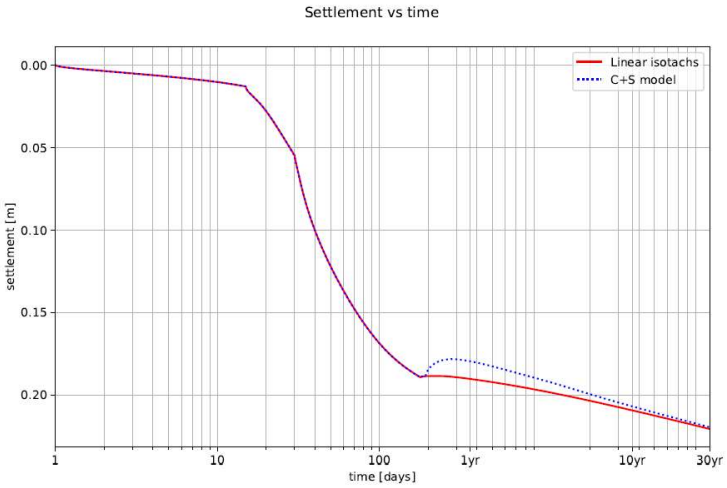

Figure 3-9, Example of settlement prediction due to embankment construction including pre-loading for linear isotachs. In the legenda linear isotachs refer to the reference implementation, C+S model is applied with linear isotachs, from: Dick (2022)

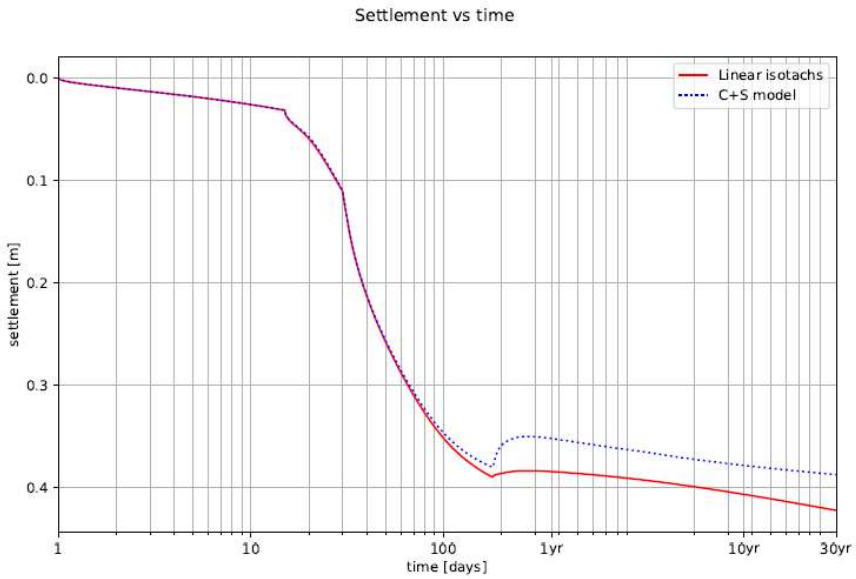

Figure 3-10, Comparison reference implementation, linear isotachs, to the C+S model, including non-linear isotachs. From: Dick (2022).

4 Summary and conclusions

The literature review shows the gradual development in the application of the isotach concept in settlement prediction. The present implementation, as described in section 2.2.1 forms a robust implementation that works well for predicting settlement due to loads that exceeds the initial yield stress and pushes subsoil conditions into the normally consolidated region. The experiences discussed in committee, see section 1.1, comply well with literature findings, Nash & Brown (2015).

When it comes to predicting settlement and creep in the over-consolidated region experimental data shows that the reference implementation, section 2.2.1, strongly underpredicts the creep rate. Section 2.2.3 and Appendix A discuss some typical results. The load steps of incremental loading tests below the natural yield stress of samples result in creep rates that are orders in magnitude higher than predicted by the reference implementation.

In recent literature non-linear isotachs, non- equally distanced, isotachs are proposed instead of linear isotachs, equally distanced, isotachs see graphs a) and b) in Figure 4-1. The reference implementation uses linear isotachs. The difference between linear and non-linear isotachs will not explain the differences observed between the experiments and reference implementation. When the distance between the isotachs reduce at lower strain rates, unloading in a field of non-linear isotachs will result in an even lower strain rate than found for linear isotachs. Non-linearity of the isotachs will not explain the trend of underestimation of the creep rate by the reference implementation.

Regarding new insights in the isotach concept, the notion of distorted isotachs, in combination with non-equally distanced isotachs might explain the difference between reference implementation and experiments, see graphs b) and c) in Figure 4-1.

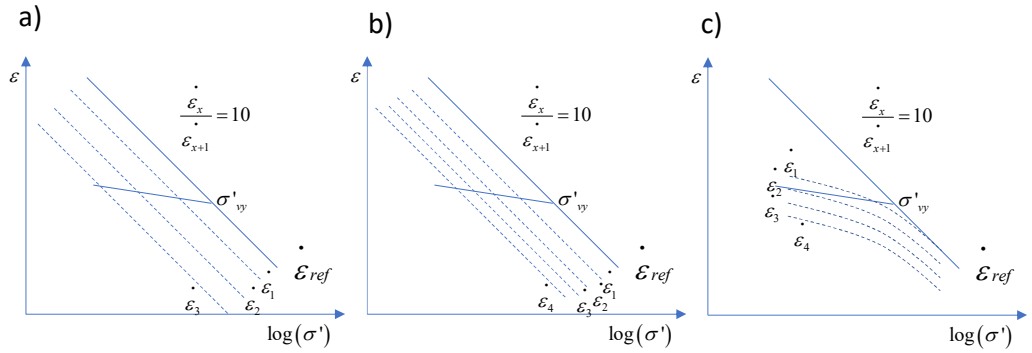

Figure 4-1, Sketch of A, linear non-distorted isotachs, B, non-linear non-distorted isotachs and C, non-linear distorted isotachs.

Nash & Brown (2015) introduces distorted isotachs for the over-consolidated region despite the origin of over-consolidation. Vergote et al. 2020, 2021 connect the distortion of the isotachs to structure changes caused by swelling during unloading. Although not explicitly discussed by the authors, for situations where over consolidation is reached by aging, Nash & Brown (2015) assumes that the initial creep strain is dictated by distorted isotachs, while in the C+S model (Vergote, 2020, 2021) predicts creep strain by non-distorted isotachs.

This has large consequences for settlement prediction for small load increments in practice. As explained in the introduction, the initial conditions play an important role in the predictions of settlement due to small load increments. Assumptions on the presence of the distortion of the isotachs has therefore consequences. Besides aging, over consolidation in de field can also be reached by small load cycles for example by ground water fluctuation.

In laboratory testing distortion of the isotachs might be explained by unloading due to sampling and sample handling. This implies that laboratory tests cannot be used to assess the initial creep strain rate in the field and as such reduces the applicability to apply laboratory test data in predicting settlement due to a small load increment.

Section 2.2.4 concludes that in the prediction of settlement due to small load increments, the initial; strain rate, or more generally the initial conditions play important role. Section 2.2.3 and appendix A seem to indicate that the reference implementation does not correctly predict the initial strain rate and therefore seems to be inaccurate to predict settlement due to a small load increment.

The non-linearity and distortion of the isotachs are the two main issues, found in literature, that differ from the reference implementation used in this report and relate to the initial conditions. The internal state variable, as defined in the MIT-SR model, allows creep strain to gradually accelerate to a certain value upon loading. If this effect represents physical behaviour, it might have an additional effect to non-linearity or distortion of isotachs. The application of non-linear isotachs causes the distance between the isotachs to decrease at lower strain rates, see Figure 4-1. For a specific unloading step, the use of non-linear isotachs will result in lower predicted strain rates then will be found when linear isotachs are used. Since the reference implementation seems to underpredict the strain rates, the use of non-linear isotachs instead of linear isotachs alone will not improve settlement predictions for small load increments. Application of distorted isotachs will result in higher strain rates in the over consolidated region and therefore might improve the ability to predict settlement due to small load increments.

Although the use of distorted isotachs models the tendency needed to bring measured and predicted strain rates closer together, both distortion and non-linearity will be studied further. Both effects are mentioned in literature to affect the initial strain rate and focussing on one aspect, while discarding the other might not improve settlement prediction satisfactorily.

In the follow up of this study the effects of non-linearity and distortion of isotachs will be further examined for Dutch organic soils. It should be noted that literature mainly focuses on silty clays. The susceptibility for creep of organic soils and the presence of fibres in peat might result in differences in observed behaviour compared to the silty clays discussed in literature. In the follow up, both organic clays and peats will be studied. The underlying hypothesis is that organic clays might be closer to the materials typically studied in international literature than peats and as such might fit better to the reported phenomena.

The follow-up study will contain incremental loading tests and constant rate of strain tests. In the incremental loading tests, the stress condition will be brought stepwise beyond the initial yield stress. A large unloading step will induce a new yield stress, which is beyond the natural yield stress observed in the field. Then a stepwise increase in load will bring the stress conditions to and beyond the yield stress. Obtaining the strain rates from the loading steps below the induced yield stress allows assessment of the distorted isotachs. Based on the assessed distorted isotachs a comparison with the predicted distortion by the C+S can be made.

The level of non-linearity of isotachs for organic soils will be studied by CRS testing. By changing the applied strain rate in CRS testing the position of the different isotachs can be established and a graph like Figure 2-9 can be produced for the tested soil. Point of attention will be the duration of these tests. There should be sufficient strain developed also for the low strain rates to clearly identify the position and slope of the individual isotachs.

Finally, field data is needed is confirm the differences between the predicted and observed strain rates for small loading steps.

References

Bjerrum L. (1967) Engineering geology of Norwegian normally-consolidated marine clays as related to settlement of buildings *Geotechnique* **17**(2) 81-118

Choi, Y. K. (1982). Consolidation behavior of natural clays. PhD thesis, University of Illinois at Urbana-Champaign, UrbanaIllinois.

Degago, S. A., Grimstad, G., Jostad, H.P., Nordal, S. & Olsson, M. (2011). Use and misuse of the isotach concept with respect to creep hypotheses A and B.

Deltares (2021) D-Settlement Embankment design and soil settlement prediction, User Manual, version 21.2, D-Settlement - Deltares

Den Haan E.J. (1992) The formulation of virgin compression of soils *Géotechnique,* vol 42, p 465-483

Den Haan E.J. (1994) A simple compression model for non-brittle soft clays and peat *PhD thesis TUDelft*

Den Haan E.J. (1999) Stress independent parameters for primary and secondary compression *in: Proceedings XIIIth International Conference on Soil Mechanics and Foundation Engineering*, New Delhi, Vol I, p 65 – 70

Den Haan E.J., Edil T.B. (1994) Secondary and tertiary compression of peat *in: Advances in understanding and modelling the mechanical mbehaviour of peat, den Haan, Termaat & Edil (eds), Balkema Rotterdam*

Den Haan E.J., Sellmeijer H.J.B. (2000) Calculation of Soft Ground with an Isotach Model *in: Soft ground technology Hanson & Termaat (eds), ASCE geotechnical special publication* no 112, June 2000

Grimstad, G. & Degago, S.A. (2010). A non-associated creep model for structured anisotropic clay (n-SAC). 7th European Conf. NUMGE, Trondheim, Norway, 3-8.

Kawabe S., Tatsuoka F. (2013) Creep characteristics of clay in one-dimensional compression with unloading / reloading cycles *in: proceedings of the 18th International Conference on Soil Mechanics and Geotechnical Engineering*, Paris

Ladd, C. C., Foott, R., Ishihara, K., Schlosser, F. & Poulos, H. G. (1977). Stress–deformation and strength characteristics. In Proceedings of the 9th international conference on soil mechanics and foundation engineering, pp. 421–494. Tokyo, Japan: Japanese Society of Soil Mechanics and Foundation Engineering.

Leroueil S. (2006) The isotach approach. Where are we 50years after its development by Professor Šuklje? *in: Proceedings of the 13th Danube-European Conference on Geotechnical Engineering*, Prof. Suklje's memorial lecture, Ljubljana 2006 pp 55-88

Mesri, G. (2009). Discussion of 'Effects of friction and thickness on long-term consolidation behavior of Osaka Bay clays' by Watabe, Udaka, Kobayashi, Tabata & Emura (2008). Soils Found. 49, No. 5, 823–824.

Nash D., Brown M. (2015) Influence of Destructuration of Soft Clay on Time-Dependent Settlements: Comparison of Some Elastic Viscoplastic Models *International Journal of Geomechanics* 15(5), DOI:10.1061/(ASCE)GM.1943-5622.0000281

Sivasithamparam, N., Karstunnen, M. & Bonnier, P. (2015). Modelling creep behaviour of anisotropic soft soils. Computers and Geotechnics, 69, 46-57.

Šuklje, L. (1957). The analysis of the consolidation process by the Isotachs method. Proc. 4th Int. Conf. Soil Mech. Found. Engng, London, 1: 200-206.

Visschedijk M. (2010) Isotachen berekeningen op een sigarendoosje *Geotechniek* juli 2010

Vergote T.A. (2020) Deformation of soils: time and strain effects after unloading *PhD thesis* National University of Singapore

Vergote T.A., Leung C.F., Chain S.C. (2020) Modelling creep and swelling after unloading load and relaxation with Bayesian updating *Géotechnique* DOI:10.1680/jgeot.20.P.106

Vergote T.A., Leung C.F., Chian S.C. (2021) Elastoviscoplastic modelling with distorted isotaches and swelling for constant strain rate and incremental loading *International journal Analytical Methods in Geomechanics* 2021;1-14 DOI:10.1002/nag.3248

Watabe, Y., Udaka, K., and Morikawa, Y. (2008). Strain rate effect on long-term consolidation of Osaka bay clay. Soils Found., 48(4), 495–509.

Watabe, Y., Udaka, K., Nakatani, Y. and Leroueil, S. (2012). Long-term consolidation behavior interpreted with isotach concept for worldwide clays. *Soils & Found*., 52(3), 449–464.

Watabe Y., Leroueil (2015). Modeling and implementation of the isotach concept for long term consolidation behaviour. *Int. J. Geomech*., 15(5). DOI: 10.1061/(ASCE)GM.1943-5622.0000270

Yuan Y., Whittle A.J. (2014) Surcharge Loading On Reduction of Secondary Compression, *2014 CREBS workshop Deltares*, Delft, powerpoint presentation

Yuan, Y.,Whittle, A., and Nash, D. (2015). Model for predicting and controlling creep settlements with surcharge loading. Deformation Characteristics of Geomaterials. 10.3233/978-1-61499-601-9-931, 931-938.

Yuan, Y., & Whittle, A.J. (2018). A novel elasto-viscoplastic formulation for compression behaviour of clays. Geotechnique 68(12), 1044, doi: 10.1680jgeot.16.P276

Watabe Y., Udaka K., Nakatani Y., Leroueil S. (2012) Long-term consolidation behavior interpreted with isotach concept for worldwide clays *Soils and Foundations* 52(3):449-464 Doi: 10.1016/j.sandf.2012.05.005

Zwanenburg C. (2017) Kruip en Zwel, laboratoriumproeven op veen uit de Bloemendaler polder, Deltares report 1220018-005-GEO-v1 (in: Dutch)

Zwanenburg C. (2017[a]) The development of a large diameter sampler *in: proceedings of the 19th international conference on soil mechanics and geotechnical engineering,* Seoul

Zwanenburg C. (2021) Lecture notes TUD

A Incremental loading tests on peat from Zegveld

In this section the results of Incremental Loading, IL, tests on peat are used to illustrate the problem of using the isotach model for the estimation of the strain rate at stress levels well below the yield stress. The deviation of the theoretically calculated strain rate from the measured strain rate at the end of load step 2 is quantified.

A.1 Data

In total 9 incremental loading, IL, oedometer tests have been performed at Deltares. The tests are performed on peat, which was retrieved from at Zegveld, near Woerden, The Netherlands. Specifications of the samples are presented in Table 4-1. All oedometer tests contained a similar number of load steps. To study the strain rates due to creep, the duration of two load steps were extended to 7 days instead of the conventional duration of 1 day. The details of the oedometer tests are presented in Table 4-2. Specimens were taken from samples retrieved by the Deltares Large Diameter Sampler, DLDS. This sampler enables to retrieve high quality block samples with a diameter of 400 mm and height of 500 mm. Details of the DLDS are presented by Zwanenburg (2017[a]).

Table 4-1: In situ depth, initial water content and initial wet weight of peat samples

Test no.	Boring	Absolute depth from top of sample [m]	Absolute depth from bottom of sample [m]	Average depth [m]	Initial water content [%]	Initial unit weight [kN/m^3]
9	DLDS1[a]	-2.68	-3.18	-2.93	587	9.57
55	DLDS1	-3.08	-3.18	-3.13	578	9.80
99	DLDS2	-3.30	-3.32	-3.31	656	9.02
67	DLDS2	-3.41	-3.43	-3.42	420	9.40
97	DLDS2	-3.41	-3.43	-3.42	585	9.58
25	DLDS1	-3.84	-3.96	-3.90	673	9.41
26	DLDS1	-3.84	-3.96	-3.90	675	9.34
42	DLDS1	-7.42	-7.54	-7.48	830	9.13
65	DLDS1	-7.66	-7.76	-7.71	843	9.60

[a] DLDS is the Deltares Large Diameter Sampler, which consists of a diameter of 400 mm and height of 500 mm.

Table 4-2: Details of the oedometer tests

Load step	Load [kPa]	Duration [days]
1	2	1
2	5	7
3	7	1
4	10	1
5	15	1
6	20	1
7	40	1
8	20	1

9	40	1
10	80	7
11	140[b]	1

[a] The first load step is used as reference to determine the initial height.
[b] Test 65 is the only exception: a load of 122 kPa was applied during the last load step.

A.2 Results

A.2.1 Strain definition

Results are presented for linear strain, ε_v and natural strains, ε_v^H, which are defined according to equation (0.36) and (0.37).

$$\varepsilon_v = \frac{\Delta u_y}{H_0} \tag{0.36}$$

$$\varepsilon_v^H = -\ln\left(1-\varepsilon_v\right) \tag{0.37}$$

In which,

Δu_y = the vertical displacement [mm],

H_0 = the initial height of the sample (~20 mm), which is measured after applying a load of 2 kPa.

A.2.2 Stress versus strain

A.2.2.1. One-day compression line

The vertical effective stress (on linear and logarithmic scale) is plotted against the linear and natural strain in the table below for all tests. The yield stress is derived from the stress strain plots and is defined as the vertical stress level at the intersection point of the linear fits on the reloading data and virgin loading data. The linear fit on the reloading data is based on the measured strain after 1 day for load step 1 and 2. The linear fit on the virgin loading data is based on the measured strain level after 1 day for the two consecutive load steps which give the highest slope $\Delta\log\left(\sigma'_v\right)/\Delta\varepsilon$.

Table 4-3: Results of the stress versus one-day strains including the linear fits.

Test	$\sigma'_v - \varepsilon_v$	$\log_{10}(\sigma'_v) - \varepsilon_v$
9	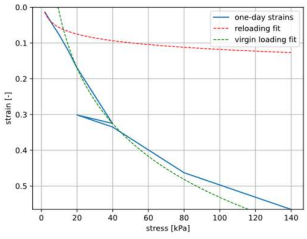	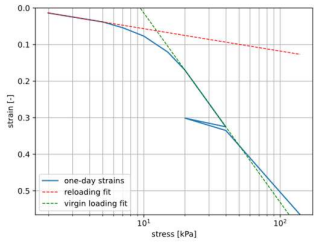

55	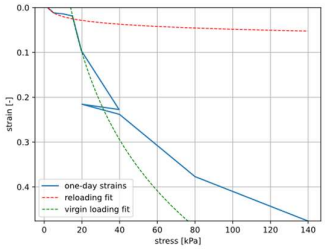 one-day strains reloading fit virgin loading fit strain [-] stress [kPa]	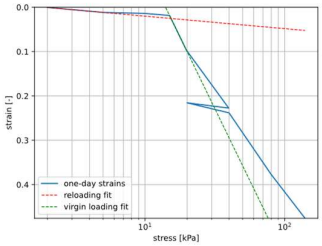 one-day strains reloading fit virgin loading fit strain [-] stress [kPa]
99	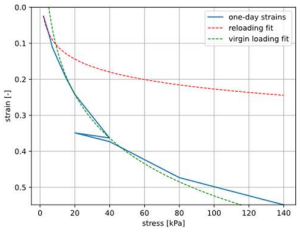 one-day strains reloading fit virgin loading fit strain [-] stress [kPa]	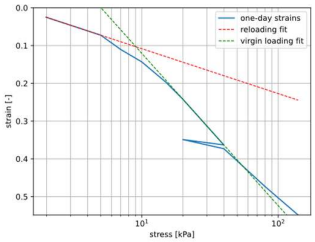 one-day strains reloading fit virgin loading fit strain [-] stress [kPa]
67	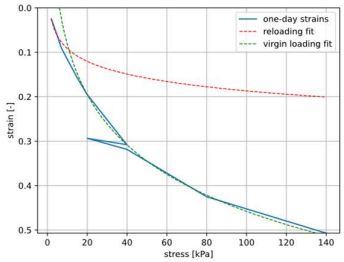 one-day strains reloading fit virgin loading fit strain [-] stress [kPa]	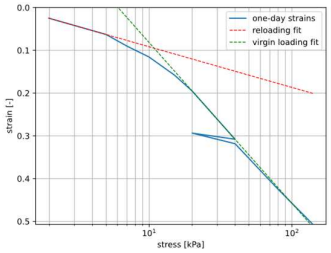 one-day strains reloading fit virgin loading fit strain [-] stress [kPa]
97	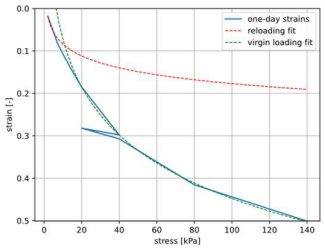 one-day strains reloading fit virgin loading fit strain [-] stress [kPa]	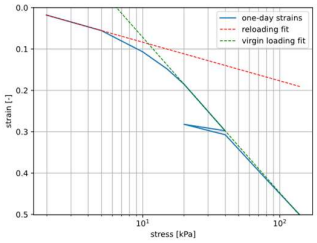 one-day strains reloading fit virgin loading fit strain [-] stress [kPa]
25	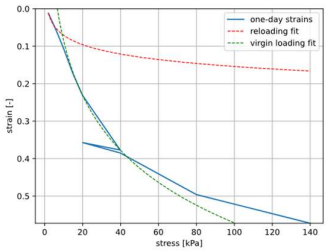 one-day strains reloading fit virgin loading fit strain [-] stress [kPa]	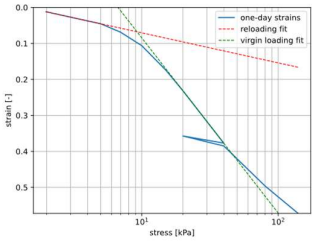 one-day strains reloading fit virgin loading fit strain [-] stress [kPa]

26	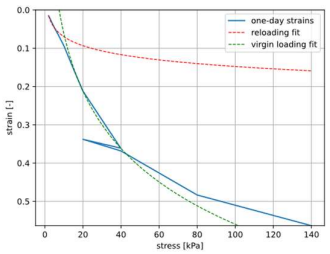	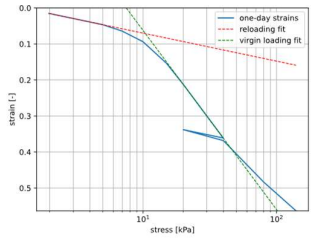
42	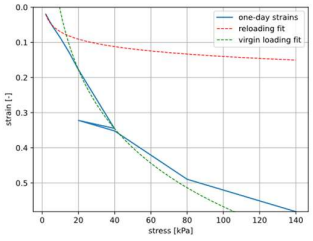	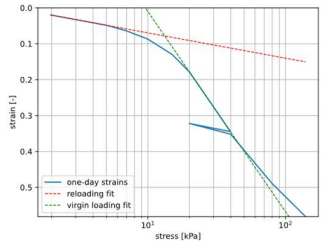
65	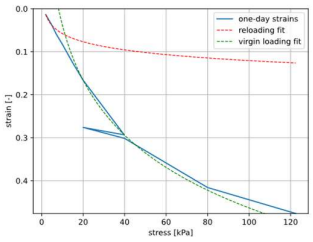	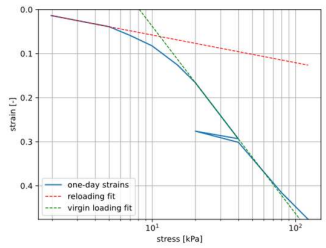

Table 4-4: Derived yield stress for all tests

Test	σ_{vy} [kPa] (linear strains)	σ_{vy} [kPa] (natural strains)
9	12.3	19.0
55	15.4	19.0
99	9.0	12.3
67	10.8	16.2
97	11.0	17.7
25	9.2	10.8
26	10.4	11.8
42	13.3	15.4
65	11.4	12.8

Table 4-5: Derived reloading and virgin loading compression ratios

Test	Linear strain			Natural strain		
	RR	RR_{ur}	CR	a	a_{ur}	b
9	0.061	0.113	0.518	0.027	0.072	0.379
55	0.028	0.075	0.648	0.012	0.042	0.310
99	0.119	0.081	0.403	0.054	0.055	0.277
67	0.095	0.083	0.376	0.043	0.052	0.274
97	0.093	0.084	0.376	0.042	0.052	0.283

25	0.083	0.093	0.487	0.037	0.064	0.305
26	0.078	0.101	0.497	0.035	0.068	0.304
42	0.071	0.100	0.558	0.032	0.065	0.356
65	0.063	0.085	0.425	0.028	0.052	0.257

A.2.2.2. Isotachs

This subsection discusses the strain rate dependency of the yield stress. The isotachs are derived from the IL tests according to the following steps:

- Load steps 4 to 7, 10 and 11 are selected with the aim of including virgin loading steps only. It must be noted that load step 4 and 5 may include (partial) reloading.
- Ordinary Least Squares (OLS) method is used to fit the time-strain data according to the relation:

$$\varepsilon = a + C_\alpha \log_{10}(t) \quad \text{(linear strains)}$$

- The OLS fit is subsequently used to calculate the strain rates with an interval of ~1 minute. The first 100 minutes of each load step are excluded, because the OLS fit cannot capture well the first part of the load step (see Section A.2.3).
- For each load step, the strains are found at a strain rate of $5 \cdot 10^{-5}$ 1/s, $1 \cdot 10^{-5}$ 1/s, $5 \cdot 10^{-6}$ 1/s, $1 \cdot 10^{-6}$ 1/s, $5 \cdot 10^{-7}$ 1/s, $1 \cdot 10^{-7}$ 1/s, $5 \cdot 10^{-8}$ 1/s.
- Finally, the isotachs can be drawn in the stress-strain space (see as example the results of Test 67 in Figure 4-2).

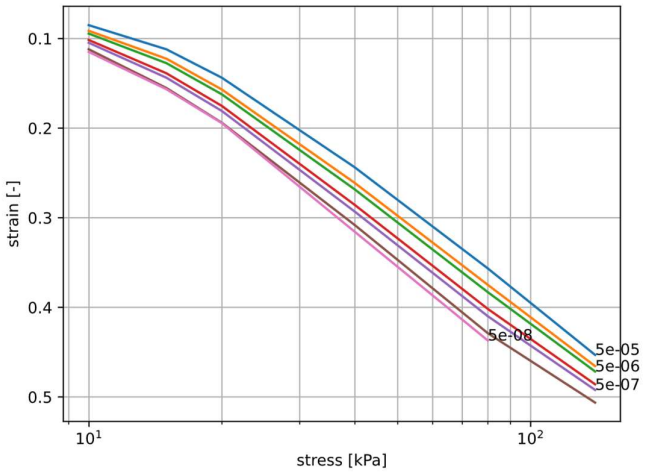

Figure 4-2: Test 67: isotachs from $\dot{\varepsilon} = 5 \cdot 10^{-5}$ s^{-1} to $\dot{\varepsilon} = 5 \cdot 10^{-8}$ s^{-1}.

For each isotach, the yield stress can be determined. The dependency of the yield stress on the strain rate is illustrated in Figure 4-3. Figure 4-3 shows the normalized preconsonsolidation pressure versus the strain rate. The normalized preconsolidation pressure is the preconsolidation pressure (σ'_{vy}) with respect to the $\sigma'_{vy,ref}$ which represents σ'_{vy} the at a strain rate of $\dot{\varepsilon} = 10^{-7} s^{-1}$. The values for $\sigma'_{vy,ref}$ are listed in Table 4-6 for all tests.

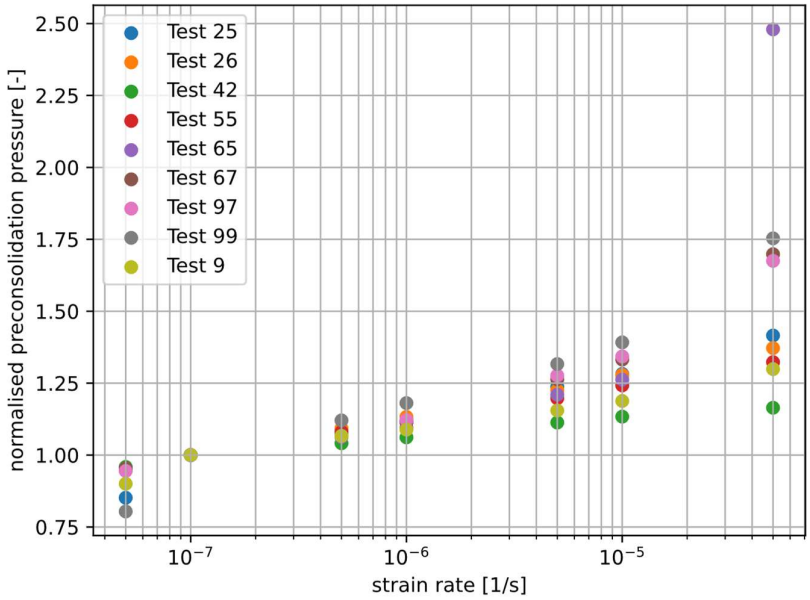

Figure 4-3: The normalized preconsolidation pressure ($\frac{\sigma_{vy}}{\sigma_{vy}(\dot{\varepsilon}=10^{-7}s^{-1})}$) versus the strain rate in s^{-1}.

From Figure 4-3, it can be observed that the yield stress tend to decease with decreasing strain rate. The spread is largest at the highest strain rates. It is very likely that consolidation was not yet completed at strain rates of $5 \cdot 10^{-5}$ s^{-1}, which results to relatively large strain increments, relatively large slopes in the logarithmic stress-strain space, and an intersection point between the reloading and virgin loading curve at higher stress levels accordingly.

Table 4-6: reference preconsolidation pressure

Test	$\sigma'_{vy,ref}$ [kPa]
9	12.5
55	15.4
99	9.2
67	12.1
97	12.5
25	9.3
26	10.4
42	13.4
65	11.5

A.2.3 Time versus strain

The non-linear least squares method is used to fit the logarithmic of the time and strain data of load step 2 and 10 to derive the creep parameter. The first 10 minutes of the load step are excluded for the fit. The plots of the raw data and fits for load step 2 and 10 are shown in Table 4-7. The creep parameter derived for all tests are listed in Table 4-8.

Table 4-7: Linear regressions on the end tail of the $log_{10}(t) - \varepsilon_v$ and $ln(t) - \varepsilon_v^H$ data points for load step 2 and 10. The logarithmic time is set to zero at the start of each load step.

Test	$\log_{10}(t) - \varepsilon_v$	$\ln(t) - \varepsilon_v^H$
9	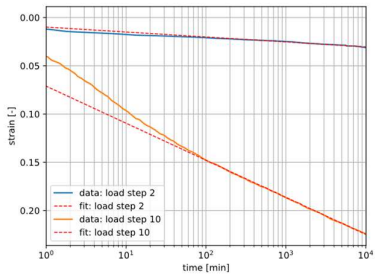	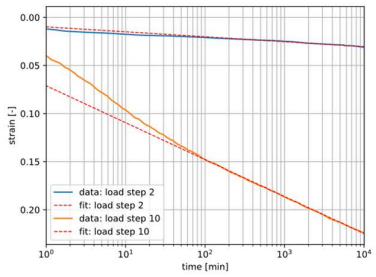
55	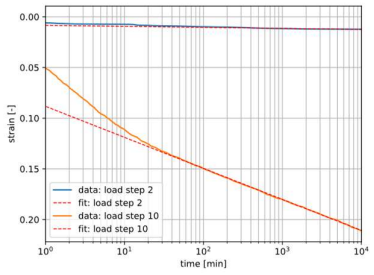	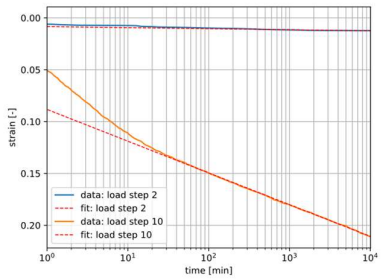
99	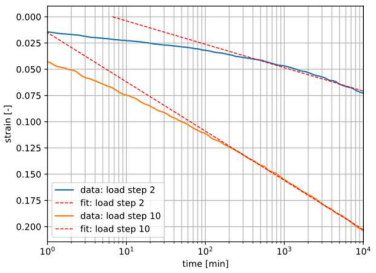	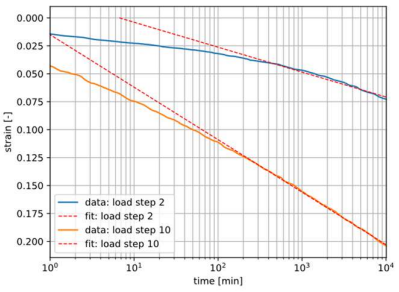
67	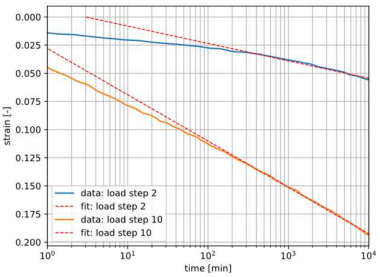	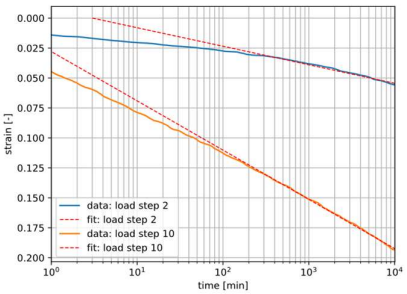

97	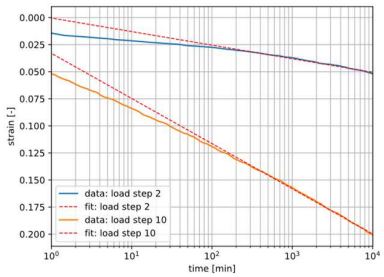 strain [-] time [min] data: load step 2 fit: load step 2 data: load step 10 fit: load step 10	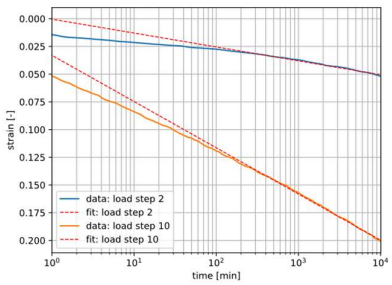 strain [-] time [min] data: load step 2 fit: load step 2 data: load step 10 fit: load step 10
25	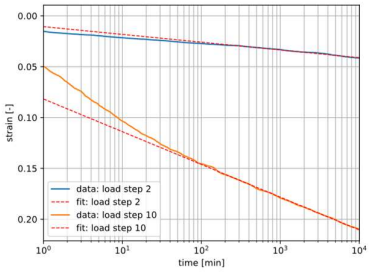 strain [-] time [min] data: load step 2 fit: load step 2 data: load step 10 fit: load step 10	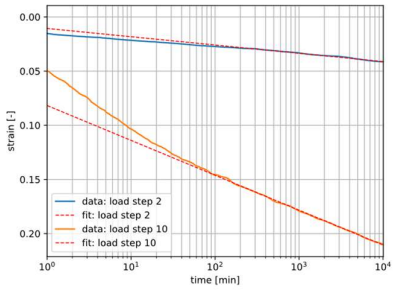 strain [-] time [min] data: load step 2 fit: load step 2 data: load step 10 fit: load step 10
26	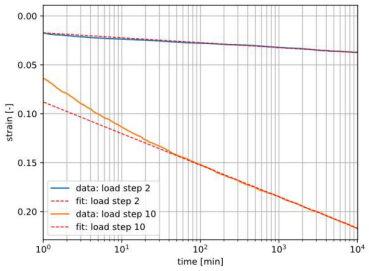 strain [-] time [min] data: load step 2 fit: load step 2 data: load step 10 fit: load step 10	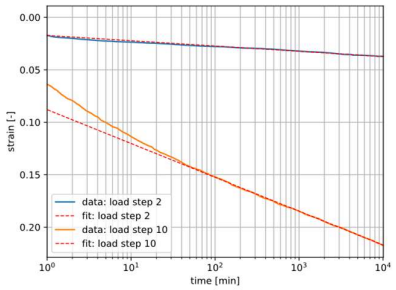 strain [-] time [min] data: load step 2 fit: load step 2 data: load step 10 fit: load step 10
42	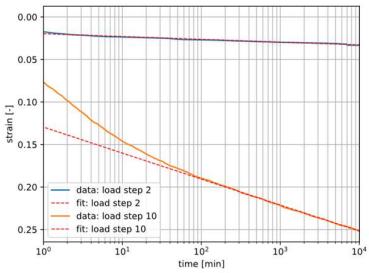 strain [-] time [min] data: load step 2 fit: load step 2 data: load step 10 fit: load step 10	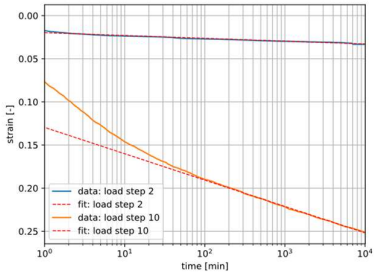 strain [-] time [min] data: load step 2 fit: load step 2 data: load step 10 fit: load step 10
65	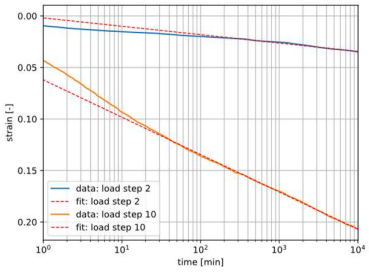 strain [-] time [min] data: load step 2 fit: load step 2 data: load step 10 fit: load step 10	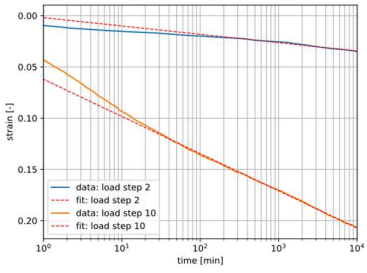 strain [-] time [min] data: load step 2 fit: load step 2 data: load step 10 fit: load step 10

Table 4-8: Slope of time – settlement curve. For normally consolidated condition in step 10 represents the creep parameter based on linear strains, C_α and natural strains, c. The R^2- value represents a measure for the quality of the fit, a perfect fit is found for $R^2 = 1.0$.

Test	Load step 2 ($5\ kPa < \sigma_{vy}$)				Load step 10 ($80\ kPa > \sigma_{vy}$)			
	$\frac{d\varepsilon_v}{d\log(t)}$	R^2 [-]	$\frac{d\varepsilon_v^H}{d\ln(t)}$	R^2 [-]	C_α [-]	R^2 [-]	c [-]	R^2 [-]
9	0.00514	0.95	0.00223	0.95	0.0384	0.98	0.01668	0.98
55	0.00101	0.78	0.00044	0.78	0.0306	0.98	0.01329	0.98
99	0.0223	0.94	0.00968	0.94	0.0470	0.97	0.02040	0.97
67	0.0155	0.95	0.00671	0.95	0.0411	0.98	0.01785	0.98
97	0.0125	0.96	0.00544	0.96	0.0417	0.97	0.01811	0.97
25	0.00765	0.95	0.00332	0.95	0.0322	0.98	0.01398	0.98
26	0.00503	0.97	0.00219	0.97	0.0323	0.98	0.01401	0.98
42	0.00328	0.84	0.00142	0.84	0.0305	0.96	0.01327	0.96
65	0.00814	0.95	0.00354	0.97	0.0363	0.98	0.01574	0.98

A.2.4 Strain rate versus strain

Table 4-9 shows the strain rates obtained from the laboratory tests with an interval of one hour from the original data set for load step 2 and 10. The curve shows the calculated strain rates according to the following equation:

$$\dot{\varepsilon} = \frac{C_\alpha}{(t - t_0)\ln(10)} \tag{0.38}$$

$$\dot{\varepsilon}^H = \frac{c}{(t - t_0)} \tag{0.39}$$

Here,
C_α = the creep parameter for linear strains derived from current load step
c = the creep parameter for natural strains derived from current load step
t_0 = the time at the start of the load step in seconds,
t = the time in seconds.

Table 4-9: The $log_{10}(\dot{\varepsilon}_v) - \varepsilon_v$ and $ln(\dot{\varepsilon_v^H}) - \varepsilon_v^H$) plots of load step 2 and 10 for all tests.

Test	$\log_{10}(\dot{\varepsilon}_v) - \varepsilon_v$	$\ln(\dot{\varepsilon_v^H}) - \varepsilon_v^H$
9	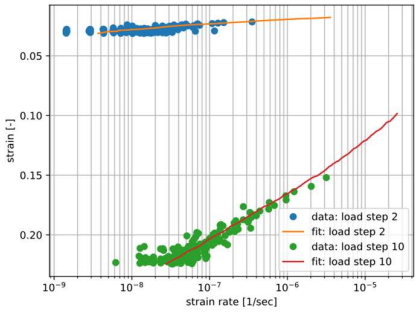	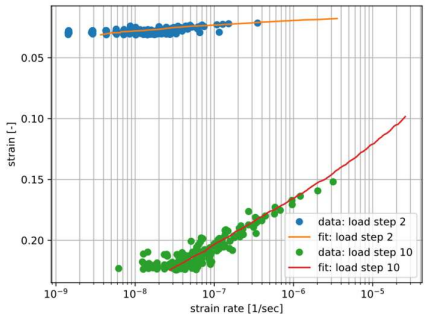
55	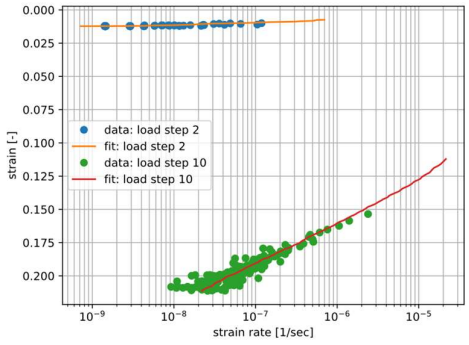	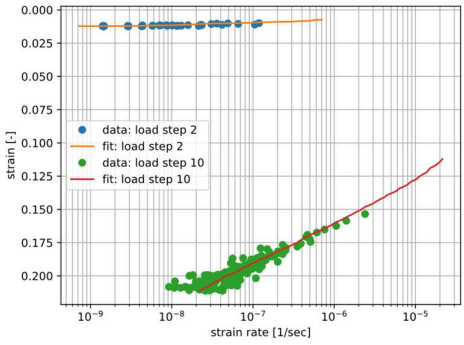
99	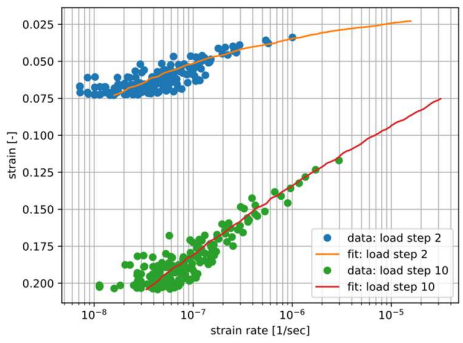	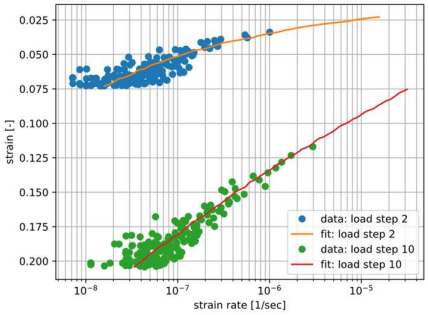
67	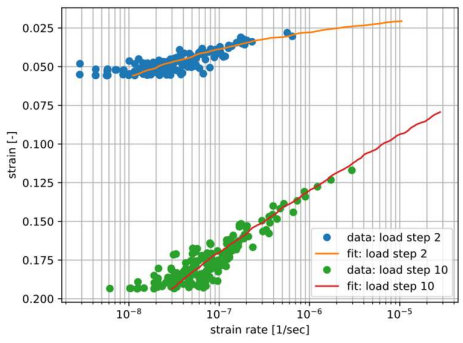	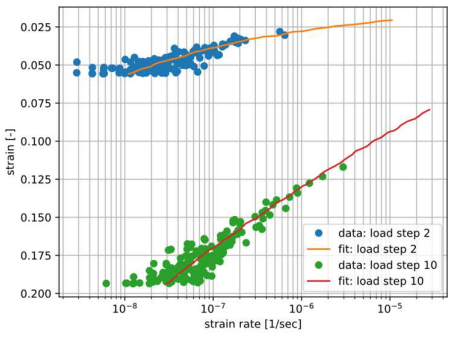

97	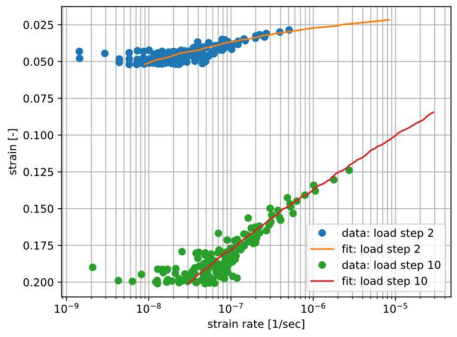 strain [-] strain rate [1/sec] data: load step 2 fit: load step 2 data: load step 10 fit: load step 10	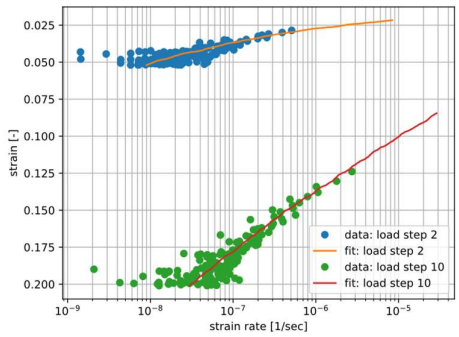 strain [-] strain rate [1/sec] data: load step 2 fit: load step 2 data: load step 10 fit: load step 10
25	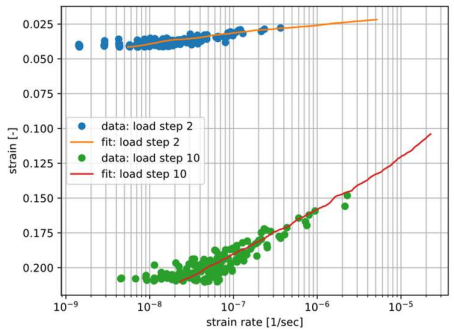 strain [-] strain rate [1/sec] data: load step 2 fit: load step 2 data: load step 10 fit: load step 10	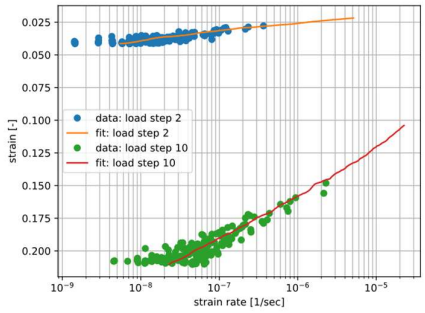 strain [-] strain rate [1/sec] data: load step 2 fit: load step 2 data: load step 10 fit: load step 10
26	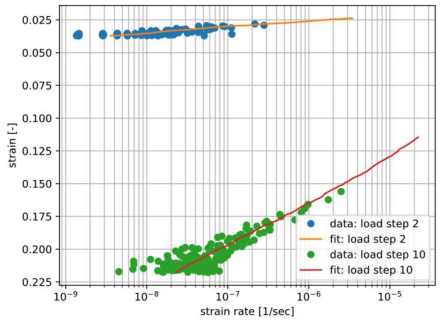 strain [-] strain rate [1/sec] data: load step 2 fit: load step 2 data: load step 10 fit: load step 10	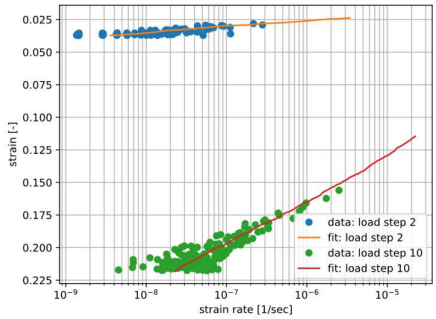 strain [-] strain rate [1/sec] data: load step 2 fit: load step 2 data: load step 10 fit: load step 10
42	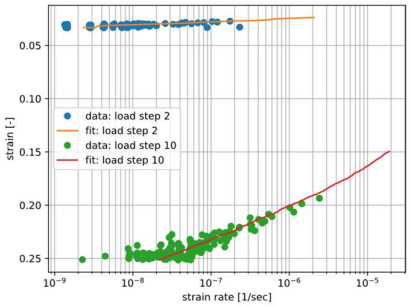 strain [-] strain rate [1/sec] data: load step 2 fit: load step 2 data: load step 10 fit: load step 10	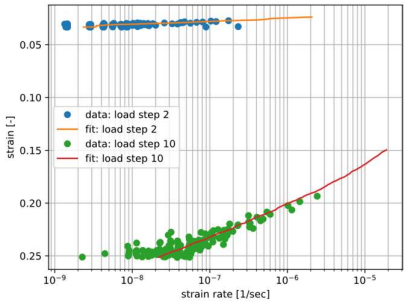 strain [-] strain rate [1/sec] data: load step 2 fit: load step 2 data: load step 10 fit: load step 10

65

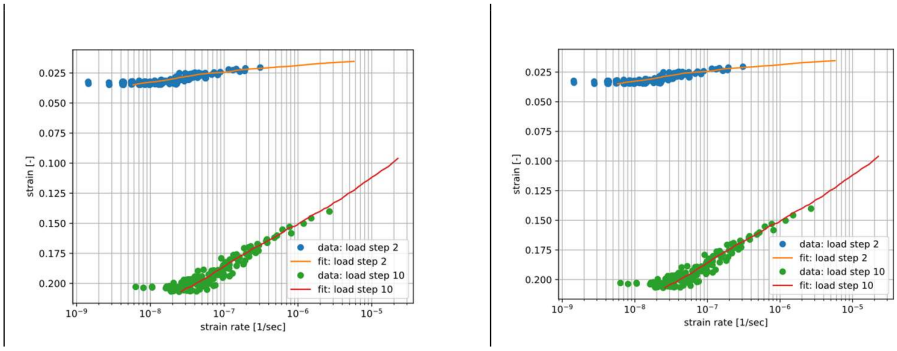

From Table 4-9, it can be observed that the scatter at the end of the load steps is quite large. Nevertheless, similar strain rates are determined at the end of load step 2 respectively load step 10 for the different tests, when using the OLS method to fit either the linear strain-time data or the natural strain-time data. Table 4-10 presents the strain rates at the end of load step 2 and 10.

Table 4-10: Strain rate at the end of load step 2 and 10.

Test	$\dot{\varepsilon}_{end}$ [1/s]		$\dot{\varepsilon}^{H}_{end}$ [1/s]	
	Load step 2	**Load step 10**	**Load step 2**	**Load step 10**
9	$3.68 \cdot 10^{-9}$	$2.75 \cdot 10^{-8}$	$3.68 \cdot 10^{-9}$	$2.75 \cdot 10^{-8}$
55	$7.24 \cdot 10^{-10}$	$2.19 \cdot 10^{-8}$	$7.24 \cdot 10^{-10}$	$2.19 \cdot 10^{-8}$
99	$1.60 \cdot 10^{-8}$	$3.36 \cdot 10^{-8}$	$1.60 \cdot 10^{-8}$	$3.36 \cdot 10^{-8}$
67	$1.11 \cdot 10^{-8}$	$2.94 \cdot 10^{-8}$	$1.11 \cdot 10^{-8}$	$2.94 \cdot 10^{-8}$
97	$8.97 \cdot 10^{-9}$	$2.98 \cdot 10^{-8}$	$8.97 \cdot 10^{-9}$	$2.98 \cdot 10^{-8}$
25	$5.47 \cdot 10^{-9}$	$2.30 \cdot 10^{-8}$	$5.47 \cdot 10^{-9}$	$2.30 \cdot 10^{-8}$
26	$3.60 \cdot 10^{-9}$	$2.31 \cdot 10^{-8}$	$3.60 \cdot 10^{-9}$	$2.31 \cdot 10^{-8}$
42	$2.35 \cdot 10^{-9}$	$2.19 \cdot 10^{-8}$	$2.35 \cdot 10^{-9}$	$2.19 \cdot 10^{-8}$
65	$5.82 \cdot 10^{-9}$	$2.59 \cdot 10^{-8}$	$5.82 \cdot 10^{-9}$	$2.59 \cdot 10^{-8}$

A.2.5 Strain rate and equivalent time: measured and analytical

The strain rate at the end of load step 2 is derived from the measurements as well as calculated according to the theory of the isotach model.

The theorical strain rate at the end of load step 2 is calculated as follows:

- The yield stress is derived as described in Section A.2.2;
- The creep parameter is derived from virgin load step 10: since the recorded time is equal to the intrinsic time for the virgin load steps;
- The intrinsic time at the start of step 2 (τ_{ini}) is calculated according to equations (0.40) and (0.41);

- The intrinsic time at the end of step 2 (τ_{end}) is equal to the intrinsic time at the start of load step 2 summed with the duration of the time step.
- The strain rate at the end of step 2 is calculated according to equation (0.42) and (0.43);

$$\tau_{ini} = OCR^{\frac{CR-RR}{C_\alpha}} \text{ (linear strains)} \quad (0.40)$$

$$\tau_{ini} = OCR^{\frac{b-a}{c}} \text{ (natural strains)} \quad (0.41)$$

$$\dot{\varepsilon} = \frac{C_\alpha}{\tau_{end} \ln(10)} \text{ (linear strains)} \quad (0.42)$$

$$\dot{\varepsilon}^H = \frac{c}{\tau_{end}} \text{(natural strains)} \quad (0.43)$$

Table 4-11: Linear strains: measured and theoretical strain rate at the end of load step 2. Test 67&97 and Test 25&26 are tests performed on a peat sample retrieved from similar in situ depth

	Test 9	**Test 55**	**Test 99**	**Test 67**	**Test 97**	**Test 25**	**Test 26**	**Test 42**	**Test 65**
σ_{vy} [kPa]	12.3	15.4	9.0	10.8	11.0	9.2	10.4	13.3	11.4
OCR [-]	2.5	3.1	1.8	2.2	2.2	1.8	2.1	2.7	2.3
$\frac{CR-RR_{ur}}{C_\alpha}$ **[-]**	10.55	18.70	6.87	7.13	7.01	12.23	12.28	14.99	9.39
τ_{start} [days]	13773	$1.34\cdot 10^{9}$	58	246	246	1656	8051	2315788	2262
τ_{end} [days]	13781	$1.34\cdot 10^{9}$	65	253	253	1663	8059	2315795	2270
$\dot{\varepsilon}_{theoretical}$ **[1/s]**	$1.4\cdot 10^{-11}$	$1.15\cdot 10^{-16}$	$3.64\cdot 10^{-9}$	$8.17\cdot 10^{-10}$	$8.28\cdot 10^{-10}$	$9.73\cdot 10^{-11}$	$2.01\cdot 10^{-11}$	$6.63\cdot 10^{-14}$	$8.03\cdot 10^{-11}$
$\dot{\varepsilon}_{measured}$ **[1/s]**	$3.68\cdot 10^{-9}$	$7.24\cdot 10^{-10}$	$1.60\cdot 10^{-8}$	$1.11\cdot 10^{-8}$	$8.97\cdot 10^{-9}$	$5.47\cdot 10^{-9}$	$3.6\cdot 10^{-9}$	$2.35\cdot 10^{-9}$	$5.82\cdot 10^{-9}$

Table 4-12: Natural strains: measured and theoretical strain rate at the end of load step 2.

	Test 9	**Test 55**	**Test 99**	**Test 67**	**Test 97**	**Test 25**	**Test 26**	**Test 42**	**Test 65**
σ_{vy} [kPa]	19.0	19.0	12.3	16.2	17.7	10.8	11.8	15.4	12.8
OCR [-]	3.8	3.8	2.5	3.2	3.5	2.2	2.4	3.1	2.6
$\frac{b-a}{c}$ **[-]**	18.41	20.11	10.88	12.45	12.78	17.21	16.84	21.89	13.07
τ_{start} [days]	$4.57\cdot 10^{10}$	$4.43\cdot 10^{11}$	$1.85\cdot 10^{4}$	$2.30\cdot 10^{6}$	$1.06\cdot 10^{7}$	$5.93\cdot 10^{5}$	$1.84\cdot 10^{6}$	$4.70\cdot 10^{10}$	$2.24\cdot 10^{5}$
τ_{end} [days]	$4.57\cdot 10^{10}$	$4.43\cdot 10^{11}$	$1.85\cdot 10^{4}$	$2.30\cdot 10^{6}$	$1.06\cdot 10^{7}$	$5.93\cdot 10^{5}$	$1.84\cdot 10^{6}$	$4.70\cdot 10^{10}$	$2.24\cdot 10^{5}$
$\dot{\varepsilon}^H{}_{theoretical}$ **[1/s]**	$4.22\cdot 10^{-18}$	$3.47\cdot 10^{-19}$	$1.27\cdot 10^{-11}$	$8.98\cdot 10^{-14}$	$1.98\cdot 10^{-14}$	$2.73\cdot 10^{-13}$	$8.80\cdot 10^{-14}$	$3.27\cdot 10^{-18}$	$8.12\cdot 10^{-13}$
$\dot{\varepsilon}^H{}_{measured}$ **[1/s]**	$3.68\cdot 10^{-9}$	$7.24\cdot 10^{-10}$	$1.6\cdot 10^{-8}$	$1.11\cdot 10^{-8}$	$8.97\cdot 10^{-9}$	$5.4714 3\cdot 10^{-9}$	$3.6\cdot 10^{-9}$	$2.35\cdot 10^{-9}$	$5.83\cdot 10^{-9}$

Table 4-13, Comparison of calculated and measured strain rate for NC conditions, step 10.

	Test 9	Test 55	Test 99	Test 67	Test 97	Test 25	Test 26	Test 42	Test 65
C_α [-]	0.0384	0.0306	0.0470	0.0411	0.0417	0.0322	0.0323	0.0305	0.0363
c [-]	0.0167	0.0133	0.0204	0.0179	0.0181	0.0140	0.0140	0.0133	0.0157
t [days]	7	7	7	7	7	7	7	7	7
$\dot{\varepsilon}^{C}_{theory}$ [10^{-8} 1/s]	2.76	2.2	3.37	2.95	2.99	2.31	2.32	2.19	2.61
$\dot{\varepsilon}^{H}_{theory}$ [10^{-8} 1/s]	2.79	2.20	3.37	2.95	2.99	2.31	2.32	2.19	2.60
$\dot{\varepsilon}_{measured}$ [10^{-8} 1/s]	2.75	2.19	3.36	2.94	2.98	2.30	2.31	2.19	2.59

A.3 Discussion

In total 9 IL-oedometer tests on peat samples from Zegveld have been conducted. The water content and densities showed that the variability between the samples was relatively small. For normally consolidated conditions, step 10 a very good agreement is found between the measured and predicted strain rates, see Table 4-13. For the over-consolidated conditions, step 2, the reference implementation underpredicts the strain rate systematically by different orders in magnitude, approximately 20 – 200. For tests 42 and 55 even larger differences are found.

Evaluation of the parameters:

- The correctness of the derived yield stress is questioned in Section A.2.2. The yield stress is derived from the logarithmic stress-strain curves. However, the yield stress cannot be traced back from the stress-strain curves on linear scale: no distinct pre-consolidated and normally consolidated behaviour can be observed. However, this parameter does not explain the large deviations in measured and theoretically calculated strain rate.
- The exponential factor $m = \frac{CR-RR}{C_\alpha}$ should be a factor 3 to 6 smaller in order to get theoretical strain rates which are in the same order of magnitude as the measured strain rates.
- The applied duration in step 2 is 7 days. The measured strain rates at the end of load step 2 correspond to intrinsic times ranging between 15-65 days, except for Test 55. The results of Test 55 would correspond to a larger intrinsic time of 213 days.

Deltares is an independent institute for applied research in the field of water and subsurface. Throughout the world, we work on smart solutions for people, environment and society.

Deltares

www.deltares.nl